ITS UCDAVIS
INSTITUTE OF TRANSPORTATION STUDIES

Research Report – UCD-ITS-RR-08-09

Calibration of CalME Models Using Field Data Collected from US 101 near Redwood National Park, Humboldt County

April 2008

Rongzong Wu

Institute of Transportation Studies ◦ University of California, Davis
1605 Tilia Street ◦ Davis, California 95616
PHONE (530) 752-6548 ◦ FAX (530) 752-6572
www.its.ucdavis.edu

April 2008
Technical Memorandum: UCPRC-TM-2008-14

Calibration of *CalME* Models Using Field Data Collected from US 101 near Redwood National Park, Humboldt County

Author:
Rongzong Wu

Partnered Pavement Research Program (PPRC) Contract Strategic Plan Element 4.1:
Development of Mechanistic-Empirical Design Method

PREPARED FOR:

California Department of Transportation
Division of Research, Innovation, and System Information (DRISI)
Office of Materials and Infrastructure

PREPARED BY:

University of California
Pavement Research Center
UC Davis, UC Berkeley

DOCUMENT RETRIEVAL PAGE	**Technical Memorandum: UCPRC-TM-2008-14**

Title: Calibration of *CalME* Models Using Field Data Collected from US 101 near Redwood National Park, Humboldt County

Author: R. Wu

Caltrans Technical Lead: Imad Basheer

Prepared for:	**FHWA No.:**	**Date Work Submitted:**	**Report Date**:
Division of Research, Innovation, and System Information Office of Materials and Infrastructure	CA139999C	August 19, 2009	April 2008

Strategic Plan No:	**Status:**	**Version No:**
4.1	Stage 6, final version	1

Abstract:
CalME is a software package under development for Caltrans that includes mechanistic-empirical response and performance models intended for the analysis and design of asphalt pavement structures. Building on existing design methods, *CalME* provides an Incremental-Recursive Mechanistic-Empirical (IRME) method in which the materials properties for the pavement are updated in terms of damage as the simulation of the pavement life progresses. The IRME design method incorporates various mathematical models to describe material behavior and predict structure performance. These models need to be calibrated before they can be used to evaluate the performance of different flexible pavement structures. Using data collected from two sites on US 101 near Redwood National Park in Humboldt County, California, this technical memorandum focuses on calibration of the incremental-recursive fatigue cracking model used in *CalME.* Fatigue shift factors of 0.075 for deterministic analysis and 0.13 for probabilistic analysis (Monte Carlo simulation) were found to best match the actual performance for the US 101 sites. These factors are quite different from those determined using accelerated pavement testing data from the WesTrack closed-circuit track and the Heavy Vehicle Simulator. More calibration studies are recommended.

Keywords:
CalME, calibration, fatigue, mechanistic-empirical

Proposals for implementation:

Related documents:
- P. Ullidtz, J. Harvey, B.-W. Tsai, C. L. Monismith. 2006. *Calibration of Incremental-Recursive Flexible Damage Models in CalME Using HVS Experiments.* UCPRC-RR-2005-06.
- P. Ullidtz, J. Harvey, B.-W. Tsai, and C.L. Monismith. 2006. *Calibration of CalME Models Using WesTrack Performance Data.* UCPRC-RR-2006-14.
- R. Wu. March 2008. *Calibration of CalME Rutting Model Using 2000 NCAT Data.* UCPRC-TM-2008-04.

Signatures:

R. Wu **First Author**	P. Ullidtz J. Signore J. Harvey **Technical Review**	D. Spinner **Editor**	J. Harvey **Principal Investigator**	I. Basheer **Caltrans Technical Lead**	T. J. Holland **Caltrans Contract Manager**

DISCLAIMER STATEMENT

This document is disseminated in the interest of information exchange. The contents of this report reflect the views of the authors who are responsible for the facts and accuracy of the data presented herein. The contents do not necessarily reflect the official views or policies of the State of California or the Federal Highway Administration. This publication does not constitute a standard, specification or regulation. This report does not constitute an endorsement by the California Department of Transportation (Caltrans) of any product described herein.

For individuals with sensory disabilities, this document is available in braille, large print, audiocassette, or compact disk. To obtain a copy of this document in one of these alternate formats, please contact: the California Department of Transportation, Division of Research Innovation, and Systems Information, MS-83, P.O. Box 942873, Sacramento, CA 94273-0001.

PROJECT PURPOSE

The study presented in this technical memorandum is part of Strategic Plan Element 4.1 of the Partnered Pavement Research Center, whose objective is to evaluate and develop mechanistic-empirical design procedures for California. The study presented in this technical memorandum provides a calibration and validation of the asphalt mix fatigue model used in *CalME,* which is the new mechanistic-empirical design software under development by UCPRC for Caltrans.

TABLE OF CONTENTS

List of Figures ..... **vii**

List of Tables ..... **ix**

1 Introduction **1**

1.1 Background 1

1.2 Objectives 2

1.3 Technical Memorandum Organization 2

2 Description of the Project Sites **3**

2.1 Overview 3

3 *CalME* Models Used **6**

3.1 Asphalt-Bound Layer Models 6

3.1.1 Material Stiffnesses 6

3.1.2 Rutting Model 7

3.1.3 Fatigue Cracking Model 8

3.2 Unbound Materials Models 11

3.2.1 Material Stiffnesses 11

3.2.2 Permanent Deformation 12

4 Data Collection **13**

4.1 Introduction 13

4.2 Environment 13

4.2.1 Temperatures 15

4.2.2 Subgrade Moisture Contents 17

4.3 Structure 17

4.3.1 Layer Thickness 18

4.3.2 Layer Moduli Backcalculation Using FWD Data 20

4.3.3 Asphalt-Bound Layer Stiffness 23

4.3.4 Unbound Layer Stiffness Model Parameters 32

4.3.5 Rutting Model Parameters for Asphalt-Bound Material 37

4.3.6 Rutting Model Parameters for Unbound Layers 38

4.3.7 Fatigue Model Parameters for Asphalt-Bound Material 38

4.3.8 Construction Variability 41

4.4 Traffic 41

4.5 Performance 44

4.6 Comparison of Model Inputs for the Two Projects 47

5 *CalME* Operation 48
5.1 Mode of *CalME* Analysis 48
5.2 Parameters to be Calibrated 48
6 Results and Discussion 49
6.1 Introduction 49
6.2 Sensitivity of the Fatigue Shift Factor for the Original HMA Surface Layer 49
6.3 Effect of Traffic Wander 51
6.4 Effect of HMA Aging 52
6.5 Effect of Traffic Speed 52
6.6 Effect of Traffic Volume 52
6.7 Sensitivity of Construction Variability 54
6.8 Determination of Fatigue Shift Factors with Deterministic Analysis 55
6.9 Determination of Fatigue Shift Factors with Probabilistic Analysis 57
6.10 Rutting Performance Validation 59
6.11 Discussion 59
7 Conclusions and Recommendations 61
References 62

LIST OF FIGURES

Figure 2.1: Locations of the MEF-2 and MEF-3 project sites. 4
Figure 2.2: Aerial view of the project area. 5
Figure 4.1: Locations of the two project sites (MEF-2 and MEF-3), along with those of the nearby weather station (Orick Prairie Creek Park Weather Station) and the weather station near the city of Arcata (Arcata/Eureka Airport Weather Station). 14
Figure 4.2: Minimum and maximum daily air temperature at the project sites. 15
Figure 4.3: Comparison of daily minimum temperatures for the two weather stations 16
Figure 4.4: Comparison of daily maximum temperatures for the two weather stations. 16
Figure 4.5: Daily precipitation for the project sites (recorded at the Orick Prairie Creek Park Weather Station). 17
Figure 4.6: DCP data and identification of layer boundary. 19
Figure 4.7: Fitting of master curve using frequency sweep data for HMA overlay at MEF-2. 25
Figure 4.8: Fitting of master curve using frequency sweep data for original HMA surface at MEF-2. 25
Figure 4.9: Fitting of master curve using frequency sweep data for HMA overlay at MEF-3. 26
Figure 4.10: Fitting of master curve using frequency sweep data for original HMA surface at MEF-3. 26
Figure 4.11: Comparison of HMA stiffnesses obtained from FS (frequency sweep) and FWD tests. 27
Figure 4.12: Comparison of FWD stiffnesses at different locations. 28
Figure 4.13: Master curves for original HMA after correction for aging. 30
Figure 4.14: Relative increase in HMA stiffness over time. 31
Figure 4.15: Lack of strong correlation is shown by variation of backcalculated AB stiffness with confinement when SG is assumed to be linear. 33
Figure 4.16: Lack of strong correlation is shown by variation of backcalculated AB stiffness with FWD drop load when SG is assumed to be linear. 33
Figure 4.17: Variation of backcalculated AB stiffness with confinement when SG is assumed to be nonlinear; compared to when SG is assumed to be linear (as in Figure 4.15), this figure shows relatively strong correlation. 34
Figure 4.18: Variation of backcalculated AB stiffness with FWD drop load when SG is assumed to be nonlinear; compared to when SG is assumed to be linear (as in Figure 4.16), this figure shows relatively strong correlation. 34
Figure 4.19: Lack of correlation is shown by variation of stiffness at the top of the SG layer with confinement effect, assuming nonlinear SG. 35
Figure 4.20: Comparison of fitted and measured normalized permanent shear strain from RSST-CH test results for HMA mix used in Goal 9 Project. 38

Figure 4.21: Comparison of stiffness reduction curves for original HMA materials sampled from MEF-2 and MEF-3 sites tested with 200 microstrain. 39
Figure 4.22: Cutting slabs of HMA layers from the pavement between wheelpaths. 40
Figure 4.23: Regression of annual average daily truck traffic count (AADTT), with a base AADTT of 430 in 1992 and a growth rate of two percent. 42
Figure 4.24: Elevation variation along US 101 near the project sites. 43
Figure 4.25: Truck speed histogram measured at the beginning of MEF-2 (PM 127.5) 44
Figure 4.26: Survey data segments available for project site MEF-2, northbound lane 2. 45
Figure 4.27: Survey data segments available for project site MEF-3, northbound lane 2. 45
Figure 4.28. Total percent wheelpath cracking for the two sites. 46
Figure 6.1: Variation of fatigue cracking life in terms of years with fatigue shift factor for the original HMA surface layer. 50
Figure 6.2: Variation of fatigue cracking life in terms of ESALs with fatigue shift factor for the original HMA surface layer. 50
Figure 6.3: Effect of wander pattern on calculated surface cracking development, FSF = 0.14 51
Figure 6.4: Effect of traffic speed on fatigue cracking life. 53
Figure 6.5: Variation of fatigue life to 10 percent wheelpath cracking with lane factor for MEF-2. 53
Figure 6.6: Empirical cumulative distribution functions of fatigue cracking life obtained from Monte Carlo simulations with different numbers of trials. 55
Figure 6.7: Comparison of calculated and observed wheelpath cracking, no wander allowed. 57
Figure 6.8: Comparison of observed cracking and ECDF for crack initiation for MEF-2 using FS stiffness for HMA layer, indicating a matching fatigue shift factor of 0.14. 58
Figure 6.9: Comparison of observed cracking and ECDF for crack initiation for MEF-3 using FS stiffness for HMA layer, indicating a matching fatigue shift factor of 0.12. 58

LIST OF TABLES

Table 2.1: Basic Project Site Information 3
Table 2.2: Design Pavement Structure of the Project Sites 3
Table 4.1. Comparison of Average Daily Minimum and Maximum Temperatures 15
Table 4.2: Layer Thicknesses for Asphalt-Bound Layers Determined from the Slabs (mm) 18
Table 4.3: Layer Thicknesses for Unbound Layers Based on FWD Backcalculation (mm) 19
Table 4.4: List of FWD Tests Conducted for the Two Projects 20
Table 4.5: Pavement Structure Combinations Used for the Layer Moduli Backcalculation 21
Table 4.6: Average Backcalculated Layer Moduli (MPa) with Coefficients of Variation 22
Table 4.7: Pavement Structure Combinations Used for the Layer Moduli Backcalculation with Nonlinear Subgrade 22
Table 4.8: Average Backcalculated Layer Moduli (MPa) and Coefficient of Variations for Nonlinear SG 23
Table 4.9: Summary of Density for Beams* Used in Frequency Sweep Tests 24
Table 4.10: Asphalt-Bound Layer Stiffness Model Parameters Used in *CalME* 24
Table 4.11: Asphalt-Bound Layer Stiffness Model Parameters After Accounting for Aging 30
Table 4.12: Measured ATPB and OGFC Resilient Modulus Reported in Reference *(10)* 31
Table 4.13: Unbound Layer Stiffness Model Parameters 36
Table 4.14: Unbound Layer Stiffness Model Parameters for WesTrack Materials 36
Table 4.15: Calculation of *CalME* Model Parameters for AB Layer 36
Table 4.16: HMA Mixes Rutting Model Parameters for Use in *CalME* 37
Table 4.17: Unbound Material Rutting Model Parameters for Use in *CalME* 38
Table 4.18: Summary of Density for Beams Used in Fatigue Tests 40
Table 4.19: HMA Layer Fatigue Model Parameters for Use in *CalME* (i.e., Equations [9] to [11]) 40
Table 4.20: Comparison of Fatigue Life for HMA Mixes Under 200 Microstrain (millions of repetitions) 40
Table 4.21: Construction Variability Determined with Available Data 41
Table 4.22: Comparison of Model Inputs for the Two Projects 47
Table 6.1: Effect of HMA Aging on Pavement Fatigue Cracking Life 52

1 INTRODUCTION

1.1 Background

In 2005, the California Department of Transportation (Caltrans) approved an issue memo titled "Adoption of Mechanistic-Empirical (ME) Pavement Design Method," which calls for the adoption of ME pavement design methodology to replace existing pavement design methods that have been in place since the 1960s.

The University of California Pavement Research Center (UCPRC) has been supporting the Caltrans effort to implement ME pavement design by working on a series of tasks since 2000, with the most recent tasks assigned to Partnered Pavement Research Center Strategic Plan Elements 4.1 and 3.4. This calibration project is part of the work plan for PPRC SPE 4.1. This work is under the technical guidance of the Pavement Standards Team, with the Division of Design originally in the lead, with that function now transferred to the Division of Pavement Management. One of the tasks of PPRC SPE 4.1 is to develop and calibrate ME flexible pavement design models. These models have been incorporated into a draft software program called *CalME*.

CalME includes three approaches to flexible pavement design: the current Caltrans procedures based on the Hveem R-value, a "classical" ME method based on the Asphalt Institute method, and an Incremental-Recursive Mechanistic-Empirical (IRME) method in which the materials properties for the pavement are updated in terms of damage as the pavement life simulation progresses. The IRME design method incorporates various mathematical models to describe material behavior and predict structure performance. These models must be calibrated before they can be used to evaluate the performance of different flexible pavement structures.

The validation and calibration of the models in *CalME* were first performed using performance data from Heavy Vehicle Simulator (HVS) tests completed by the UCPRC between 1995 and 2004. The results of that work are documented in a report titled "Calibration of Incremental-Recursive Flexible Damage Models in *CalME* Using HVS Experiments" *(1)*. The models were next validated and calibrated using backcalculated responses and performance data from the Federal Highway Administration's full-scale closed-circuit test track project commonly referred to as "WesTrack." The validation and calibration of *CalME* using WesTrack data was performed in 2005 and 2006 *(2)*, after the validation and calibration of *CalME* models with HVS data. Additional validation and calibration is underway using data from two more full-scale closed-circuit–track accelerated pavement testing programs: the MnROAD (Minnesota DOT) and NCAT (National Center for Asphalt Technology) tracks in Minnesota and Alabama, respectively. The high-quality data and fully documented traffic, climate, and materials properties provided by HVS testing and track testing make it possible to calibrate the response and performance models in *CalME*. The accelerated nature of HVS testing and track testing means that the models in *CalME* still need to be verified with field observations to make sure the difference in field testing and accelerated testing are accounted for properly.

This document is one of a series of technical memorandums and reports documenting analysis of field section data using *CalME*, comparison of predicted and actual performance, and adjustment of transfer functions in the models to better predict actual performance.

1.2 Objectives

This technical memorandum documents the calibration of the incremental-recursive fatigue model used in *CalME* using data collected from two locations on US 101 near Redwood National Park in Humboldt County, California. This section is commonly referred to as the "Redwood Park Bypass" and was constructed in the 1990s to replace an original section of US 101 that goes through the national park in northern Humboldt County. The rutting model could not be calibrated because no rutting was observed in the field and no rutting data were measured as part of the Caltrans Pavement Condition Survey. However, rutting performance was predicted with the *CalME* models as a check on the reasonableness of the models for this location where little rutting occurred.

CalME is currently under continuous development. The *CalME* used in this calibration study is Version 0.8-20080701, posted on June 9, 2008.

1.3 Technical Memorandum Organization

This technical memorandum presents a summary of the model calibration study and is organized as follows:

- Chapter 2 provides brief descriptions of the project site.
- Chapter 3 presents models used by *CalME* in the study.
- Chapter 4 presents and discusses the collection of the necessary data for running *CalME.*
- Chapter 5 presents details on how *CalME* was run to simulate field performance.
- Chapter 6 provides results and discussions.
- Chapter 7 presents conclusions reached from the calibration study.

2 DESCRIPTION OF THE PROJECT SITES

2.1 Overview

The sites chosen for calibrating *CalME,* which are located on northbound US 101 in Humboldt County, California, have two lanes in each direction. Basic information on the two project sites is listed in Table 2.1. The two sites are only 2.4 miles apart but their elevations differ by 779 ft (237 m). The sites are located on an ascending segment of US 101 with no exits or ramps between them. The overall locations for the two sites are shown in Figure 2.1, and an aerial view of the project area is shown in Figure 2.2. These two sites will be referred to as "US 101 MEF" sites, indicating "mechanistic-empirical design for flexible pavements."

Table 2.1: Basic Project Site Information

Site Name	Starting Postmile on US 101	Lane Number	Elevation	Starting GPS Coordinates
MEF-2	Humboldt County 1+27.5	2 (truck lane)	513 ft	41°21.579' N, 124°00.213W
MEF-3	Humboldt County 1+29.9	2 (truck lane)	1,292 ft	41°22.931' N, 123°59.718W

The pavements at the two sites share the same construction history, have the same design structure (shown in Table 2.2), and the same hot-mix asphalt (HMA) base and subbase materials. The purpose of the Redwood National Park Bypass Project was to enhance travel on US 101 and to reduce conflicts between through traffic and park users. In 1992, the State of California completed the 12-mile bypass (PM Humboldt 125.8 to 137.1) of Prairie Creek Redwoods State Park and the Redwood National Park on US 101 in northern Humboldt and southern Del Norte Counties *(http://www.cahighways.org/097-104.html#101).* The entire project received an asphalt overlay in 2002. Note that only the structure built before the overlay in 2002 was used in this calibration; see Chapter 4 for more details.

Table 2.2: Design Pavement Structure of the Project Sites

Layer Number	Layer Type	Description	Year Opened to Traffic	Thickness (mm)
1	HMA Wearing Course	OGFC, PBA-6a binder	2002	25
2	HMA Overlay	HMA, Type A, PBA-1 binder (AR4000)	2002	75
3	Original HMA Surface	HMA, Type B, AR4000 binder	1992	140
4	ATPB base	AR8000 binder	1992	75
5	AB and AS	Aggregate base and subbase, Class 2	1992	405
6	SG	SC-SM, Silty, clayey sand with gravel	1992	-

Judging from the soil samples taken from the field, soil classifications of the aggregate base (AB) and aggregate subbase (AS) for MEF-2 were both GP-GC (i.e., poorly graded gravel with silty clay and sand), and for MEF-3 they varied from SW-SC (i.e., well-graded sand with silty clay and gravel) to GW-GC (i.e., well-graded gravel with silty clay and sand).

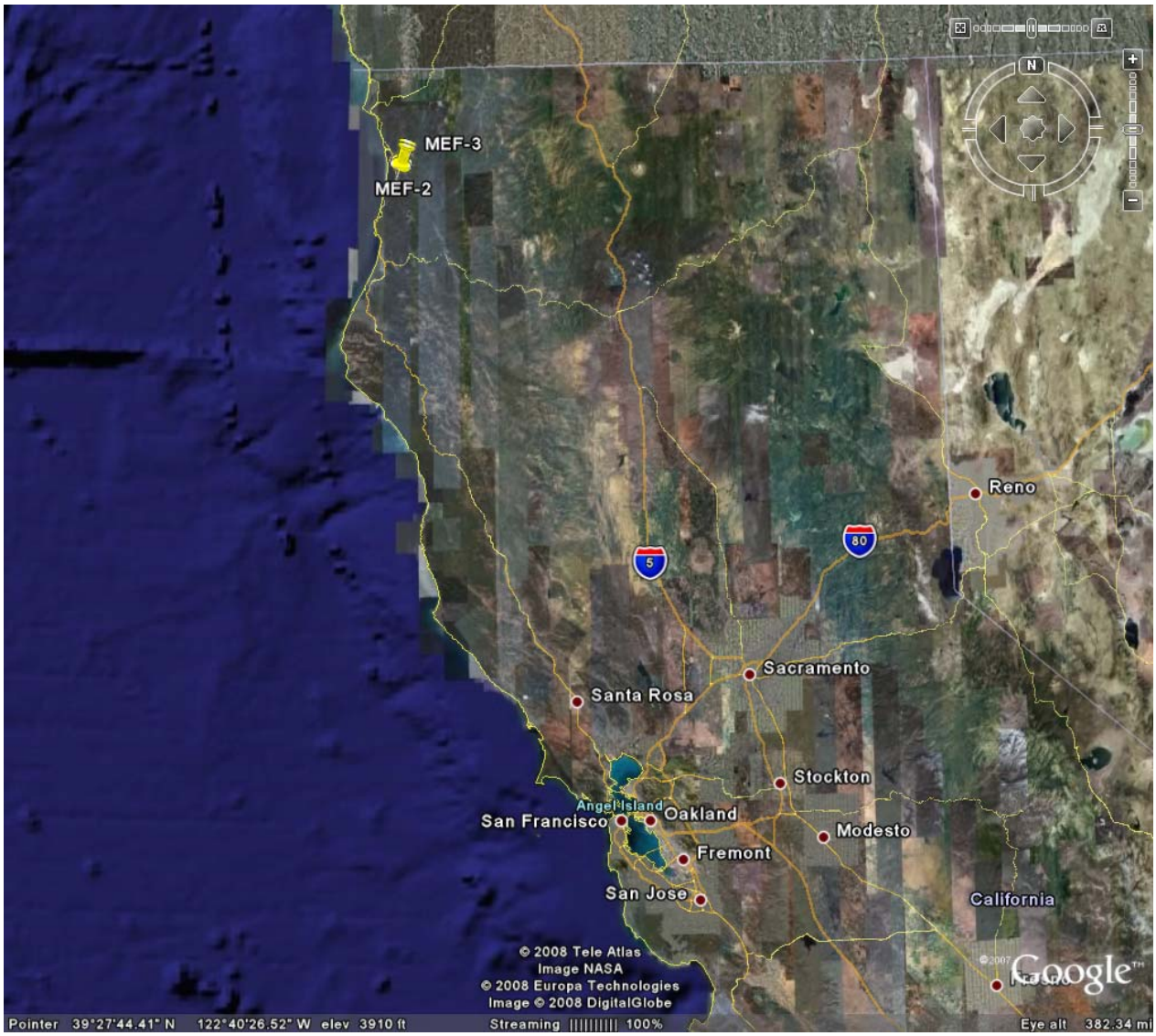

Figure 2.1: Locations of the MEF-2 and MEF-3 project sites.
(Generated using *Google Earth.*)

Figure 2.2: Aerial view of the project area.
(Generated by *Google Earth.*)

3 *CALME* MODELS USED

This chapter describes the theoretical approach used to model various components of the pavement in *CalME* for this study. Note that the models may change in future versions of the software. These models are described in the help file *CalME_Help_File.chm* and *CalME.pdf* in the *CalME* installation folder, which typically is named *C:\Program Files\CalME*.

Both rutting and fatigue models are used in this study. Although the rutting model could not be positively calibrated since there was no surface rutting observed at the project sites, it can be validated if it predicts very little rutting. On the other hand, the surface cracking development history recorded by the Caltrans Pavement Condition Survey was extracted from the Caltrans PMS database, which allows calibration of the fatigue cracking model used in *CalME*.

3.1 Asphalt-Bound Layer Models

The US 101 MEF sites both include asphalt-bound materials in their top four layers (see Table 2.2). The *CalME* models used in this study include those for stiffness, rutting, and fatigue.

3.1.1 Material Stiffnesses

The asphalt-bound materal modulus is modeled in *CalME* as a function of temperature and loading time, using the National Cooperative Highway Research Program (NCHRP) 1-37A Design Guide model *(3)*:

$$\log(E) = \delta + \frac{\alpha}{1+\exp(\beta+\gamma\log(tr))} \quad \textbf{(1)}$$

where E is the modulus in MPa,
tr is reduced time in sec,
α, β, γ, and δ are constants, and
logarithms are to base 10.

Reduced time is found from:

$$tr = lt \times \left(\frac{visc_{ref}}{visc} \right)^{aTg} \quad \textbf{(2)}$$

where *lt* is the loading time (in sec),
$visc_{ref}$ is the binder viscosity at the reference temperature,
visc is the binder viscosity at the present temperature, and
aTg is a constant.

and the binder viscosity can be calculated from temperature using the following equation:

$$\log(\log visc\ cPoise) = A + VTS \cdot \log T_k \quad \textbf{(3)}$$

where T_k is binder temperature in Kelvin, and A = 9.6307 and VTS = -3.5047.

In the version of *CalME* used for this study, aging is accounted for using the following equation:

$$E(d) = E(d_0) \times \frac{A \cdot \ln(d) + B}{A \cdot \ln(d_0) + B} \quad \textbf{(4)}$$

where $E(d)$ and $E(d_0)$ are the stiffness at day d and d_0 after construction, respectively, and A, B are constants.

Setting d_0 to 1, the above equation leads to:

$$E(d) = E(1) \times \left[\frac{A}{B} \cdot \ln(d) + 1 \right] \quad \textbf{(5)}$$

which indicates that aging is really determined by the ratio between A and B only; therefore it is safe to assume B as 1.0.

It should be noted that δ in Equation (1) is typically fixed at 2.30, indicating a fixed value for a minimum stiffness of 200 MPa (29 ksi), based on backcalculated results from the HVS and WesTrack calibrations of *CalME*.

3.1.2 Rutting Model

A shear-based approach developed by Deacon et al. *(4)* for predicting rutting of the asphalt layer was used. Rutting in the asphalt is assumed to be controlled by shear deformation. The rutting estimates used computed values of shear stress, τ, and elastic shear strain, γ^e, at a depth of 50 mm (2 in.) beneath the edge of the tire. It is also assumed in this approach that rutting occurs solely in the top 100 mm (4 in.) of the HMA layer.

Rutting in the HMA layer due to the shear deformation is determined from the following:

$$rd_{AC}\ mm = K \times \gamma^i \times h \quad \textbf{(6)}$$

where $rd_{AC}\ mm$ is the vertical rut depth in the asphalt concrete,
γ^i is the permanent (inelastic) shear strain at 50 mm depth,
K is a value relating permanent shear strain to rut depth (mm), and
h is the thickness of the HMA layer in millimeters, with a maximum value of 100 mm.

The permanent strain may be calculated from a gamma function:

$$\gamma^i = \exp\left(A + \alpha \times \left[1 - \exp\left(-\ln(N)/\gamma \right) \times \left(1 + \ln(N)/\gamma \right) \right] \right) \times \exp\left(\beta \times \tau / \tau_{ref} \right) \times \gamma^e \qquad \textbf{(7)}$$

where τ = shear stress determined at this depth using elastic analysis,
γ^e = corresponding elastic shear strain (m/m),
N = equivalent number of load repetitions, which is the number of load repetitions at the stress and strain level of the next time increment to reach the permanent shear strain calculated at the end of current time increment, and
A, α, β, γ, and τ_{ref} are constants.

3.1.3 Fatigue Cracking Model

Damage in asphalt-bound materials that is caused by fatigue appears at the pavement surface as longitudinal or transverse cracks in the wheelpath, and these cracks eventually join to form alligator cracking. In *CalME*, the density of surface cracking caused by fatigue is a function of the damage in an asphalt-bound layer. The fatigue damage, in turn, is accumulated at a rate that is determined by the tensile strain caused by traffic loading. Fatigue damage determines the residual stiffness of asphalt-bound materials. Specifically, the modulus for asphalt-bound material with damage ω becomes:

$$\log(E) = \delta + \frac{\alpha \times (1 - \omega)}{1 + \exp(\beta + \gamma \log(tr))} \qquad \textbf{(8)}$$

where the variables are defined in Equation (1) and the damage ω is calculated from:

$$\omega = \left(\frac{MN}{MN_p} \right)^{\alpha} \qquad \textbf{(9)}$$

where MN is the number of load applications in millions,
MN_p is the allowable number of load repetitions in millions, and
α is a material dependent exponent. α is calculated using the following equation:

$$\alpha = \exp\left(\alpha_0 + \alpha_1 \times \frac{t}{1°C} \right) \qquad \textbf{(10)}$$

where t = material temperature in °C, and
α_0 α_1 are material constants

while MN_p is calculated using the following equation:

$$MN_p = A \times \left(\frac{\varepsilon}{\varepsilon_{ref}} \right)^{\beta} \times \left(\frac{E}{E_{ref}} \right)^{\gamma} \times \left(\frac{E_i}{E_{ref}} \right)^{\delta} \quad \textbf{(11)}$$

where ε = bending strain at the bottom of the asphalt layer, με,
ε_{ref} = reference bending strain, με,
E_i = intact modulus for the current temperature and loading time,
E_{ref} = reference modulus, and
A, β, γ, and δ are material constants.

The model parameters for Equations (9) to (11) are determined by fitting the stiffness reduction curves from bending beam fatigue tests. If all of the parameters are allowed to vary, the resulting damage model leads to unreasonable predictions of field performance. Specifically, hot weather is much more damaging than cold weather, and most of the damage will occur in the summer. Therefore, it was decided to apply the following restrictions on the parameters while this issue is being investigated: $\alpha_1 = 0$, $\delta = 0$, and $\gamma = \beta/2$. By setting $\alpha_1 = 0$, α in Equation (10) is no longer a function of temperature. Setting $\delta=0$ removes the effect of intact stiffness E_i in Equation (11) and further removes the effect of temperature on fatigue damage because intact stiffness is temperature dependent. Setting $\gamma = \beta/2$ is a strategy adopted to reduce the number of model parameters and to introduce the concept of strain energy as the main factor controlling the rate of fatigue damage since strain energy is defined as the product of stress and strain:

$$U = \varepsilon \cdot \sigma = \varepsilon \cdot E \cdot \varepsilon = \varepsilon^2 \cdot E \quad \textbf{(12)}$$

With the restrictions $\alpha_1=0$, $\delta=0$, and $\gamma=\beta/2$, Equation (11) can be further simplified as:

$$MN_p = A \times \left(\frac{U}{U_{ref}} \right)^{\gamma} \quad \textbf{(13)}$$

It should be noted that fatigue damage is not the relative decrease in modulus. In fact:

$$\omega = \frac{\ln(E / E_i)}{\ln(E_{\min} / E_i)} = \frac{\ln(SR)}{\ln(E_{\min} / E_i)} \quad \textbf{(14)}$$

where $E_{\min} = \exp(\delta)$ is the minimum modulus (δ is the one defined in Equation [1]). As shown in the above equation, the actual relative decrease in modulus will depend on the minimum modulus, E_{min}, and on the intact modulus, E_i, which again is a function of temperature and loading time. For example, a decrease in modulus by 50 percent would correspond to a damage value between 0.15 and 0.30 if E_{min} = 100 MPa, depending on the initial modulus.

Once the fatigue damage for the asphalt surface layer has been determined, the surface crack density can be calculated. The amount of cracking at crack initiation must be assumed (in calibration studies, values of 5 percent of the wheelpath [WesTrack sections]) or 0.5 m/m^2 [HVS sections] have been used).

$$CR = \frac{A}{1 + \left(\frac{\omega}{\omega_0} \right)^{\alpha}} \quad \textbf{(15)}$$

where CR = Surface crack density, either in percent area or m/m^2, and
A, ω_0 and α are constants.

In *CalME*, A = 100% and α= –8 in Equation (15) based on WesTrack data. When using the percent area definition, the calculated crack density CR can be treated as the percent wheelpath cracked. The value of ω_0 depends on the asphalt layer thickness and *CalME* backcalculates its value based on a known pair of values for damage ω and crack density CR. This is done by calculating the damage ω corresponding to crack initiation and assuming that crack density corresponding to crack initiation is 5 percent wheelpath cracked or a crack density of 0.5m/m^2. The damage to the surface layer at crack initiation is, in turn, determined from

$$\omega_{initiation} = \frac{1}{1 + \left(\frac{h_{HMA}}{h_{ref}} \right)^{a}} \quad \textbf{(16)}$$

where $\omega_{initiation}$ = fatigue damage when crack initiation occurs,
h_{HMA} = surface HMA layer thickness,
h_{ref} = reference value for surface HMA layer thickness, and
a is a constant.

In *CalME*, a = –2 and h_{ref}= 250 mm based on WesTrack data, which was determined based on the performance of sections with the Fine Superpave mix and the Fine Plus Superpave mix.

Surface crack densities calculated using the above equations are based on deterministic simulations in which input parameters have fixed values. This method was used to perform sensitivity studies. An alternative method based on probabilistic simulations are used to perform the actual calibration. In the probabilistic simulations, layer thicknesses and stiffnesses are allowed to vary based on predefined statistical distributions for subsections of the pavement section. Monte Carlo simulations are conducted to obtain empirical cumulative density functions for crack initiation time, which is then compared with the observed wheelpath cracking history. Details of these analyses are presented in Chapter 6.

3.2 Unbound Materials Models

Three types of unbound materials are present in the US 101 MEF sites: Class 2 aggregate base, Class 2 aggregate subbase, and the subgrade.

3.2.1 Material Stiffnesses

Unbound materials are treated as linear elastic material with a Poisson's ratio of 0.35. During calibration of the *CalME* models using data from the first 27 flexible HVS test sections and the 26 original WesTrack sections, it was found that the moduli of unbound materials could vary with the stiffness of the asphalt layers. This occurred both when the variation in stiffness was due to temperature variations and when it was due to fatigue damage to the asphalt. The change in stiffness was the opposite of what would be expected for granular layers due to the nonlinearity of the material. The following relationship is used to describe this stiffness variation as a function of confinement in the unbound layers from the layers above them:

$$E_n = E_{n,ref} \times \left[1 - \left(1 - \frac{S^3}{S_{ref}^3} \right) \times StiffnessFactor \right] \quad \textbf{(17)}$$

where: E_n is the modulus of layer n,
$E_{n,ref}$ is the modulus of layer n at a bending stiffness $S = S_{ref}$, and
S_{ref} and *Stiffness factor* are constants.

And the bending stiffness S for layer n is calculated as:

$$S = \sum_{1}^{n-1} h_i \times \sqrt[3]{E_i} \quad \textbf{(18)}$$

where: h_i is the thickness of layer i, counting from the surface, and
E_i is the modulus of layer i.

The unbound layers for some of the HVS tests also showed the well-known nonlinearity of granular materials, with the modulus of granular layers increasing with increasing bulk stress and the modulus of cohesive materials decreasing with increasing deviator stress. In *CalME,* this nonlinearity is treated as a function of the wheel load rather than as a function of the stress condition to avoid the interdependence between stiffness and stress:

$$E_P = \left(\frac{P}{40kN} \right)^{\alpha} \times E_{40kN} \quad \textbf{(19)}$$

where: E_P is the modulus at wheel load P in kN,
$E_{40\,kN}$ is the modulus at a wheel load of 40 kN, and
α is a constant (positive for granular materials and negative for cohesive).

Combining Equations (17) and (19) leads to the following complete model for unbound layer stiffness:

$$E = E_{n,ref} \times \left[1 - \left(1 - \frac{S^3}{S_{ref}^3} \right) \times StiffnessFactor \right] \cdot \left(\frac{P}{40kN} \right)^{\alpha} \quad \textbf{(20)}$$

3.2.2 Permanent Deformation

Permanent deformation, d_p, of the unbound materials is based on the vertical resilient strain at the top of the layer, ε, and on the modulus of the material, E:

$$d_p = A \times MN^{\alpha} \times \left(\frac{\varepsilon}{\varepsilon_{ref}} \right)^{\beta} \times \left(\frac{E}{E_{ref}} \right)^{\gamma} \quad \textbf{(21)}$$

where d_p= permanent deformation (mm) of an unbound layer,
MN = number of load repetitions in millions, and
A, α, β, γ, ε_{ref}, and E_{ref} are constants.

As with the asphalt layer, rutting in unbound layers is assumed to have occurred in the upper part of each layer. The difference is that for unbound layers the thickness of the upper part of the unbound layer over which this occurs is unknown, and as a result there is no thickness in Equation (21). As a result, the model was calibrated without explicit input for unbound layer thickness.

4 DATA COLLECTION

4.1 Introduction

The data needed for *CalME* calibration can be grouped into four major categories: environment, traffic, structure, and performance. The first three data groups provide necessary inputs for running *CalME,* while the last group provides measured results for use in calibrating empirical shift factors used in *CalME* so that the calculated performance can match the measured values.

This chapter describes how the model parameters were determined, using various sources of data collected. The UCPRC crew conducted a field trip to the two sites on March 28, 2007, to collect data and bring back materials for laboratory testing. The data collected from both field and laboratory testing include:

- Construction history and structure information provided by the Caltrans District Materials Engineer, Dave Waterman;
- Performance history extracted from the Caltrans pavement management system (PMS) database;
- Falling-weight deflectometer (FWD) testing conducted by the UCPRC crew during the field trip;
- Bending beam fatigue and frequency sweep testing on structural HMA layers using beams cut from slabs taken from the site by the UCPRC crew;
- Results from repeated simple shear test at constant height (RSST-CH) conducted for the HVS Goal 9 *(5)* Project on HMA mix, which is a material similar to the ones used in the structural HMA layers for the two MEF sites, based on binder type, mix type, and air-void contents;
- Dynamic Cone Penetrator (DCP) testing data on aggregate base and subgrade conducted by the UCPRC crew;
- Traffic data extracted from the statewide Weigh-in-Motion (WIM) database for California provided by UCPRC and the Caltrans traffic statistics website, and a one-day Caltrans traffic data survey measured with a portable WIM at the project site; and
- Climate data from the National Climatic Data Center (NCDC).

4.2 Environment

Environmental conditions refer to the temperatures of the pavement and the moisture contents of both aggregate base and subgrade. These conditions affect layer stiffnesses. *CalME* can use pavement temperatures precalculated with the software program *Enhanced Integrated Climate Model (EICM) (6)* for various pavement structures and different climate zones in California. Once a user specifies the correct climate zone for a given project, *CalME* will use a precalculated surface temperature to determine in-depth temperatures based on the selected pavement structure.

Geographically, the project sites are in the "North Coast" climate zone, whose pavement temperatures were calculated based on data collected by a weather station located in the city of Arcata, which is only 35 miles from the project. Accordingly, the climate zone for the two project sites was chosen to be the "North Coast." To verify the accuracy of this designation, air temperatures and precipitation measured by a weather station near the project site (the Orick Prairie Creek Park [OPCP] Weather Station) were compared to those measured by one near Arcata (the Arcata/Eureka Airport [AEA] Weather Station). The locations of the project sites and those of the two weather stations are shown in Figure 4.1.

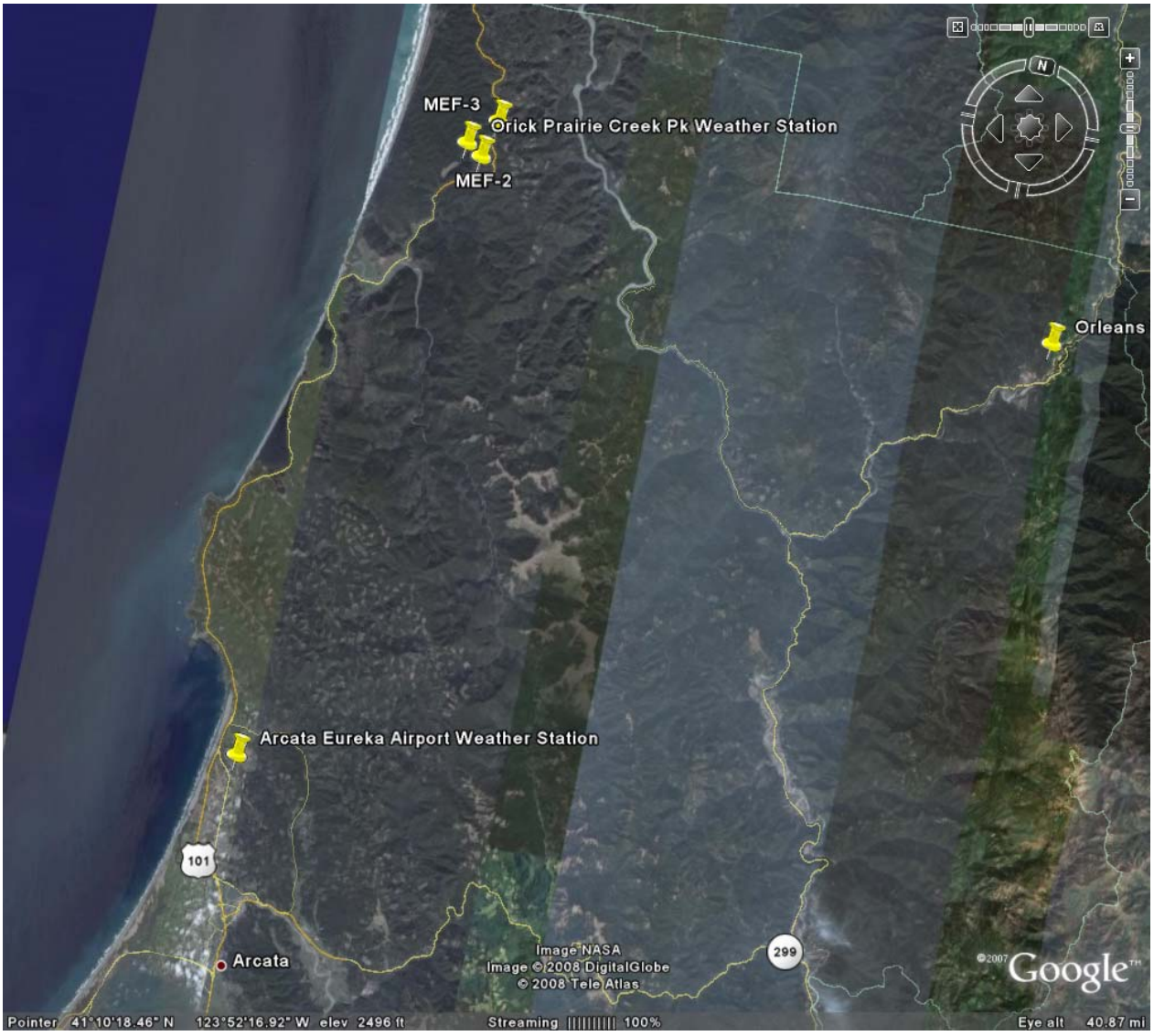

Figure 4.1: Locations of the two project sites (MEF-2 and MEF-3), along with those of the nearby weather station (Orick Prairie Creek Park Weather Station) and the weather station near the city of Arcata (Arcata/Eureka Airport Weather Station).
(Generated by *Google Earth.)*

4.2.1 Temperatures

The daily minimum and maximum temperatures for the project sites are shown in Figure 4.2, according to the records for the OPCP weather station. The temperatures are mostly between zero and 25°C, with an average daily temperature variation of about 10°C.

Comparisons of daily minimum and maximum temperatures for the OPCP and AEA weather stations are shown in Figure 4.3 and Figure 4.4, respectively. The figures show that temperatures at the OPCP station were not consistently higher/lower than those at the AEA station. The average daily minimum and maximum temperatures are shown in Table 4.1, which again shows a negligible difference between the stations. It is therefore concluded that using temperature data for the "North Coast" region is appropriate.

Table 4.1. Comparison of Average Daily Minimum and Maximum Temperatures

Weather Station	Average Daily Minimum	Average Daily Maximum
Orick Prairie Creek Park	5.9°C	16.4°C
Arcata Eureka Airport	7.3°C	15.9°C
Difference	-1.4°C	0.5°C

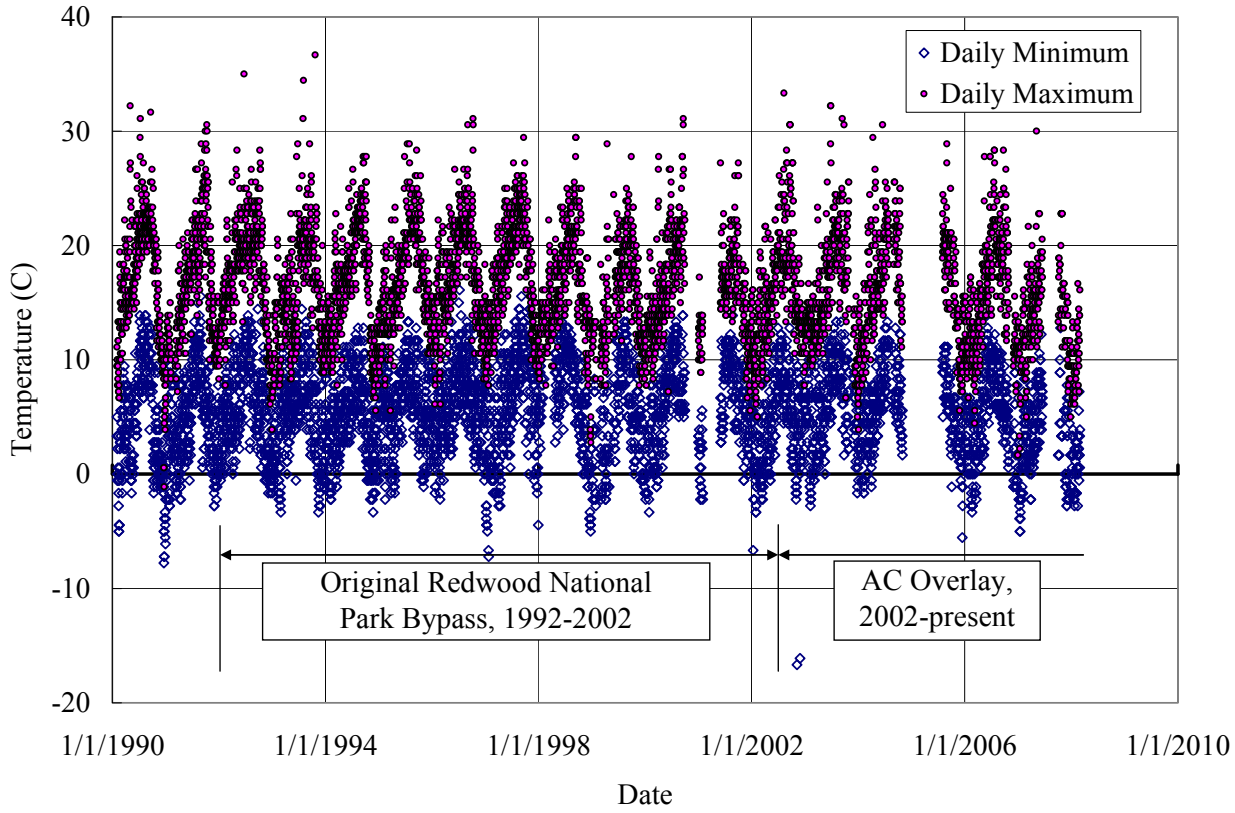

Figure 4.2: Minimum and maximum daily air temperature at the project sites.

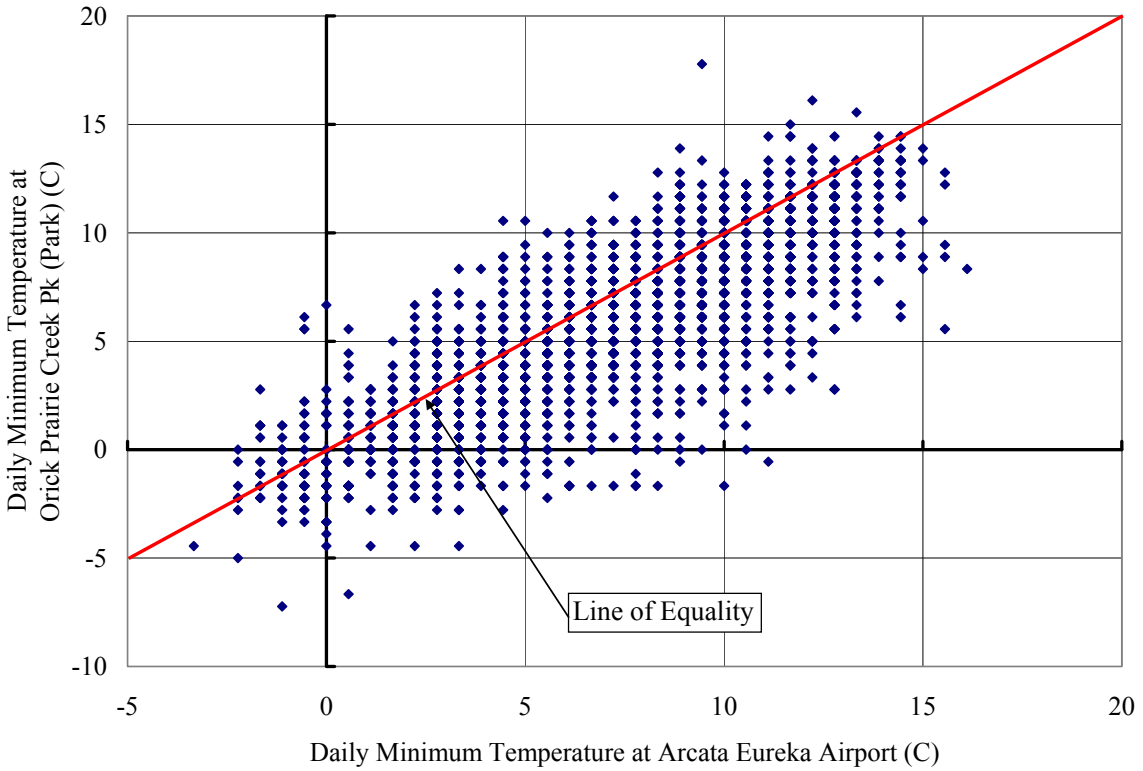

Figure 4.3: Comparison of daily minimum temperatures for the two weather stations

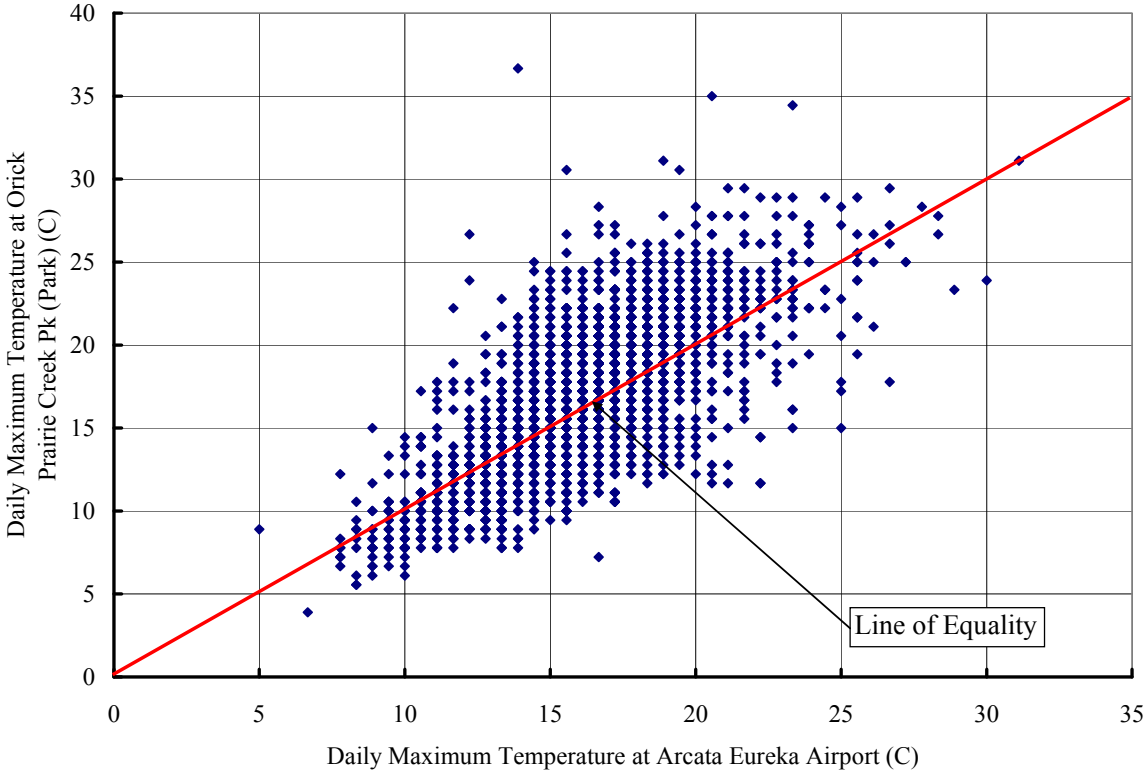

Figure 4.4: Comparison of daily maximum temperatures for the two weather stations.

4.2.2 Subgrade Moisture Contents

No soil moisture sensor data were available for the two project sites. The daily precipitation for the project sites is shown in Figure 4.5. As shown in the figure, most of the precipitation occurs in the winter and spring (September to March). Preliminary analysis of FWD data from around the state *(7)* indicates that seasonal stiffness changes of subgrade and unbound layers are highly dependent on drainage and agricultural and other practices near each project. Based on this information, the parameters controlling the seasonal variation of the unbound layers' stiffnesses in the current version of *CalME* have been set to result in constant values since no data is available to justify a more detailed evaluation. Note however that the current version of *CalME* allows for sinusoidal yearly variation of unbound material moduli to account for moisture changes in them.

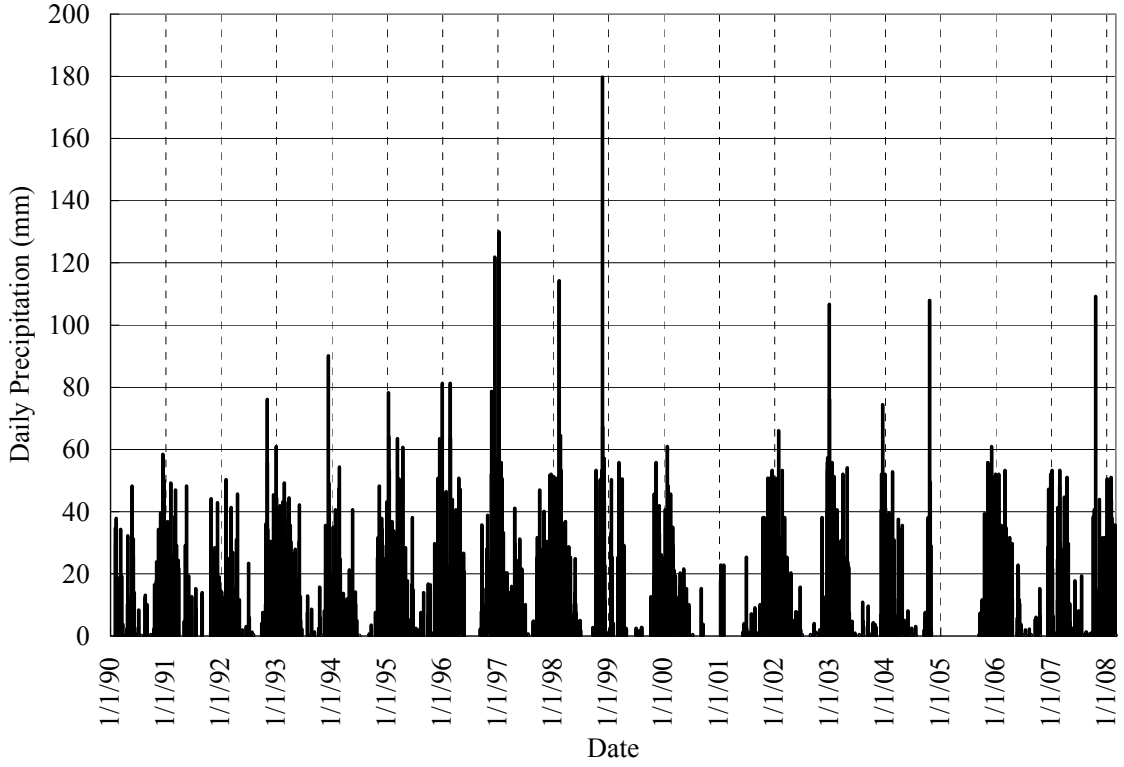

Figure 4.5: Daily precipitation for the project sites (recorded at the Orick Prairie Creek Park Weather Station).

4.3 Structure

Structure parameters include layer thicknesses and the mechanical properties of materials used in the pavements. Layer thicknesses were determined based on the original designs as well as from measurements taken in the field. The stiffnesses of various layers were determined from various sources of data, including results from frequency sweep tests in the lab and FWD and DCP tests in the field. Fatigue and permanent deformation model parameters were obtained from laboratory test results.

4.3.1 Layer Thickness

The design layer thicknesses for the two project sites are the same and are listed in Table 2.2. The as-built HMA layer thicknesses were also measured from slabs taken out of the actual pavement, with the average values shown in Table 4.2. According to the table, the measured thicknesses for the asphalt-bound layers are roughly the same as the design values; it was therefore decided to use the design thicknesses for *CalME* simulations as well as for layer moduli backcalculations.

Table 4.2: Layer Thicknesses for Asphalt-Bound Layers Determined from the Slabs (mm)

Layer Number	Layer Name	MEF-2	MEF-3	Design
1	OGFC	21	25	25
2	HMA Overlay	73	81	75
3	Original HMA	138	140	140

The actual thickness for the ATPB layer could not be measured from cores and was assumed to be the same as the design thickness, i.e., 75 mm (3 in.).

DCP tests were conducted on the underlying granular layer (aggregate base and subbase combined) and subgrade after the HMA slabs were taken out. One DCP test was done for each MEF site. The drop count data are plotted in Figure 4.6, which indicates that there are three distinct layers below the ATPB at MEF-2 and two layers at MEF-3 based on the change in penetration rate. For MEF-2 there are two layer boundaries, one at 300 mm depth and another at 600 mm depth. This indicates that there is 300 mm of well-compacted granular material (which should be the combined AB and AS layer) followed by 300 mm of softer material, with stiffer material below that. For MEF-3, there is only one layer boundary, at 400 mm depth, indicating a stiffer 400 mm granular layer below the ATPB, with softer material below that—which is closer to the combined AB and AS of 405 mm that the design layer thicknesses suggest should be present.

In many projects, the thicknesses of unbound layers may have large variations in the field. In fact, the large difference in DCP results between MEF-2 and MEF-3 indicates that such large variation in unbound layer thicknesses does exist in the two MEF sites since these two sites share the same design structure. Accordingly, the layer thicknesses determined from a single DCP test should not be regarded as applicable to a long section of pavement.

On the other hand, FWD tests were conducted at various points along the pavement and provide a more comprehensive description of the pavement structure. If layer thicknesses assumed in layer moduli backcalculation are not reasonable, the backcalculation results tend to be unreasonable as well. This provides a method for choosing reasonable thicknesses for unbound layers.

During layer moduli backcalculation for the two projects, several combinations of unbound layer thicknesses were tried before the final values were chosen. The trial thickness combinations are given based on DCP results. The combination of unbound layer thicknesses found to yield reasonable layer moduli are listed Table 4.3. Details of the layer moduli backcalculation will be presented in the Section 4.3.2.

Table 4.3: Layer Thicknesses for Unbound Layers Based on FWD Backcalculation (mm)

Layer Number	Layer Name	MEF-2	MEF-3	Design
5	Aggregate Base and Subbase (AB + ASB)	405	405	405
6	Top of Subgrade (TSG)	300	300	-
7	Remaining Subgrade (RSG)	0	0	-

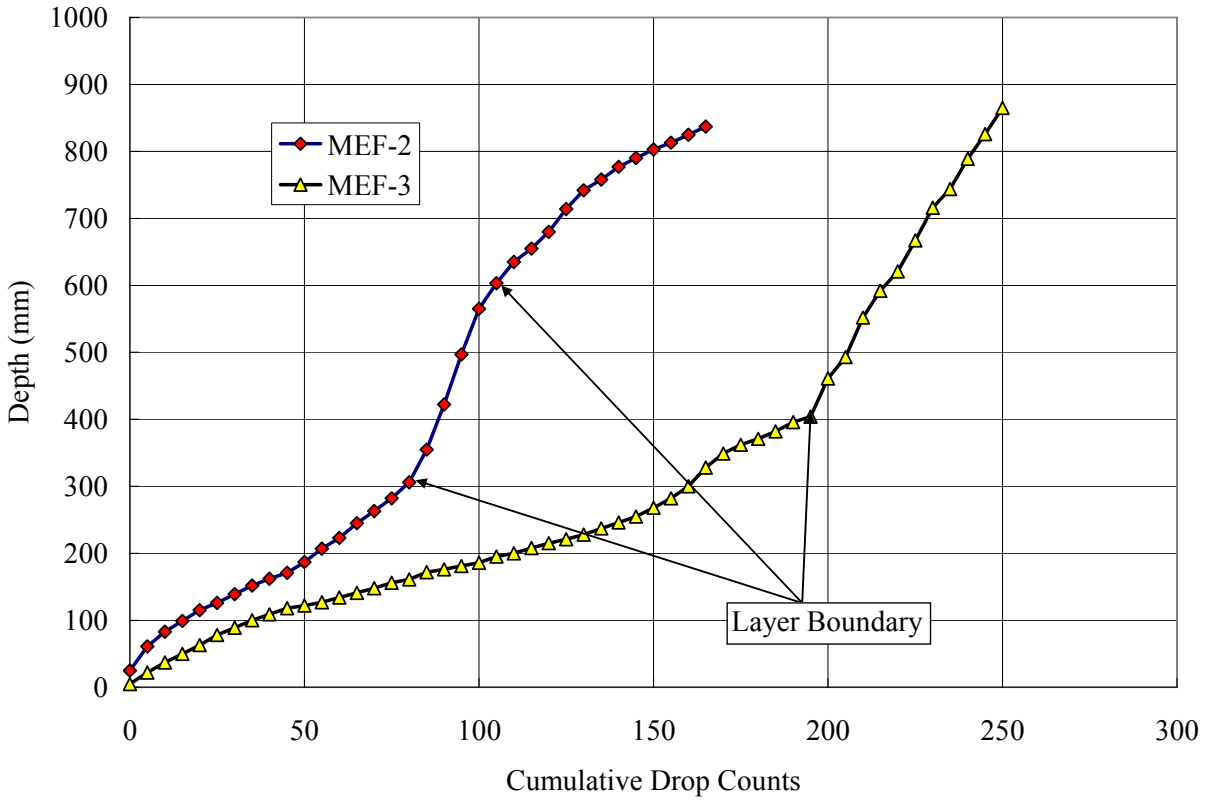

Figure 4.6: DCP data and identification of layer boundary.

4.3.2 Layer Moduli Backcalculation Using FWD Data

FWD tests were conducted twice for each project site, once in the morning and once around noon. Further, each time FWD testing was conducted along both the right wheelpath and between the wheelpaths. The list of FWD tests conducted for the two sites is shown in Table 4.4. The testing was conducted at four load levels: 30, 40, 50, and 60 kN, although the actual load used can be off by 5 kN. Testing was done mostly at a 2-m interval, although 1- to 3-m intervals were used as well. At each station, eight drops were performed with two drops for each load level. Eight geophones were used to collect surface deflections but only the first seven were used in the backcalculation because the last geophone was too far (1,975 mm) from the loading plate.

To allow for direct comparison of backcalculated layer moduli between drops in the wheelpath and those between wheelpaths, the timing of FWD tests were specially arranged so that pavement temperatures were roughly the same when tests were done along these two lines. For example, the morning session of FWD tests between wheelpaths for MEF-2 was broken into two sequences (No. 1 and 3 in Table 4.4), with FWD testing along the right wheelpath (No. 2 in Table 4.4) conducted in between. The pavement temperatures at station –8 to +10 did not change when FWD tests No. 1 and No. 2 were done.

Table 4.4: List of FWD Tests Conducted for the Two Projects

Test Number	Site	Wheelpath	Date	Time	Stations (m)	Surface Temperature
1	MEF-2	Between	3/28/07	8:45~9:16	-8~+10	2°C~5°C
2	MEF-2	Right	3/28/07	9:20~10:26	-8~+50	2°C~9°C
3	MEF-2	Between	3/28/07	10:32~11:10	+12~+50	6°C~15°C
4	MEF-3	Between	3/28/07	11:45~12:03	-5~+6	11°C~13°C
5	MEF-3	Right	3/28/07	12:10~13:12	-5~+50	12°C~21°C
6	MEF-3	Between	3/28/07	13:22~14:16	+8~+50	18°C~23°C
7	MEF-3	Between	3/29/07	9:00~9:19	+6~+14	6°C~10°C
8	MEF-3	Right	3/29/07	9:20~9:48	+6~+14	6°C~8°C
9	MEF-2	Between	3/29/07	11:24~11:31	+42~+50	19°C~24°C
10	MEF-2	Right	3/29/07	11:34~11:41	+42~+50	20°C~26°C

To limit the number of unknowns in the layer moduli backcalculation, OGFC and ATPB layer stiffnesses were fixed at given values during the process. Several combinations of stiffness were tried for each of the two layers. Specifically, OGFC layer stiffness was set at 1,000, 2,000 and 3,000 MPa, while ATPB layer stiffness was set at 1,000 or 500 MPa. OGFC was set to be stiffer than ATPB to account for the aging effect on OGFC and because ATPB layers tend to deteriorate in the field due to stripping.

Several combinations of thicknesses for unbound layers were also tried. Note that subgrade stiffness tends to increase with depth due to various factors. A simple strategy to capture this variation is to subdivide the SG into two sublayers: the top 300 mm (abbreviated as TSG, top of SG) and the remaining semi-infinite subgrade (abbreviated as RSG, remaining SG). The unbound layers therefore consist of three layers: AB, TSG, and RSG. Based on DCP data, the following values of layer thickness combination triplets (AB, TSG, RSG) were tried: (405 mm, 300 mm, 0 mm), (300 mm, 300 mm, 0 mm). In addition, backcalculations were also conducted without subdivision of the SG layer, i.e., AB thickness was set to either 405 mm or 300 mm and SG was set to be semi-infinite.

In total, there were 24 combinations of fixed quantities, including OGFC and ATPB layer stiffness and AB and SG layer thicknesses. The structures used to perform backcalculation are listed in Table 4.5.

Table 4.5: Pavement Structure Combinations Used for the Layer Moduli Backcalculation

Layer Number	Description	Stiffness** (MPa)	Thickness** (mm)
1	OGFC	1,000, 2,000, 3,000	25
2	HMA Overlay + Original HMA Surface	Variable	75+140
3	ATPB	500, 1,000	75
4	Aggregate Base (AB)	Variable	300, 405
5	Top of Subgrade (TSG)*	Variable	0, 300
6	Remaining Subgrade (RSG)	Variable	-

*: TSG layer may not be present for some combinations.
** Values used for final analysis are underscored.

Deflection data for all drops were used for backcalculation. Once backcalculations were completed for all of the thickness and stiffness combinations, one combination was chosen to represent the whole project. The criteria for choosing a particular combination were:

1. The selected combination should provide an excellent match between calculated and measured deflection bowls, which means that the root mean square (RMS) of error should be as small as possible;
2. The backcalculated layer moduli should be reasonable: AB and SG stiffness should be less than 1,000 MPa and preferably below 500 MPa.

The underscored values in Table 4.5 indicate the final combination of fixed inputs chosen. The average backcalculated layer moduli are listed in Table 4.6. According to the table, between wheelpaths moduli are generally higher than the right wheelpath moduli, which is reasonable since damage caused by trafficking is

mostly limited to the wheelpaths. Furthermore, damage mostly occurred in the HMA, AB, and TSG layers for MEF-2 and in the HMA, AB, and RSG for MEF-3. It is also important to note that there are significant variations in the layer moduli for the AB and TSG layers along the sections, which may be due to unmeasured thickness changes as much as stiffness changes.

Table 4.6: Average Backcalculated Layer Moduli (MPa) with Coefficients of Variation

Layer Name	MEF-2		MEF-3	
	Between[X]	Right[X]	Between[X]	Right[X]
Combined HMA layer (HMA)	8,761 (0.16)*	7,236 (0.20)	8,049 (0.25)	7,387 (0.16)
Aggregate Base (AB)	447 (0.29)	368 (0.37)	416 (0.32)	364 (0.32)
Top of Subgrade (TSG)	104 (0.43)	77 (0.49)	149 (0.40)	141 (0.43)
Remaining Subgrade (RSG)	441 (0.15)	455 (0.16)	500 (0.15)	445 (0.15)

[X]: Between indicates "Between wheelpaths" and Right indicates "Right wheelpath."
*: Values are reported with average moduli along with coefficient of variability in parentheses.

The typical way to deal with increasing SG stiffness over depth in the backcalculation software program *CalBack* is to use the following nonlinear model:

$$E = C \cdot \left(\frac{\sigma_1}{p_a} \right)^n \quad \textbf{(22)}$$

where: E is the SG modulus,
σ_1 is major principle stress from the external loading, and
C and n are constants and p_a is the atmospheric pressure for normalization.

Backcalculation using a nonlinear subgrade was also tried. In this case, the pavement structure used for backcalculation is listed below in Table 4.7. Note that the layers have been combined, and for this case the combined thickness for the ATPB and AB layer was set to 400 mm to get more reasonable results.

Table 4.7: Pavement Structure Combinations Used for the Layer Moduli Backcalculation with Nonlinear Subgrade

Layer Number	Description	Stiffness (MPa)	Thickness (mm)
1	OGFC + HMA Overlay + Original HMA Surface	Variable	25+75+140
2	ATPB + Aggregate Base (AB)	Variable	400
3	Subgrade (SG)	Variable and nonlinear	0

The average backcalculated layer moduli are listed in Table 4.8. In contrast to when SG is assumed to be linear (Table 4.6), when SG is assumed to be nonlinear, the stiffness at the top of the subgrade (i.e., TSG) is roughly the same, but the HMA stiffness is lower and the AB stiffness is higher.

Table 4.8: Average Backcalculated Layer Moduli (MPa) and Coefficient of Variations for Nonlinear SG

Layer Name	MEF-2		MEF-3	
	Between[X]	Right[X]	Between[X]	Right[X]
Combined HMA layer (HMA)	6,032 (0.12)*	5,118 (0.15)	5,701 (0.17)	5,216 (0.13)
Aggregate Base (AB)	700 (0.14)	596 (0.21)	693 (0.26)	613 (0.26)
Top of Subgrade (TSG)	122 (0.19)	88 (0.24)	159 (0.26)	140 (0.23)
Nonlinear factor *n* for SG	-0.31 (-0.19)	-0.40 (-0.19)	-0.28 (-0.34)	-0.28 (-0.33)

[X]: Between indicates "Between wheelpaths" and Right indicates "Right wheelpath."

*: Values are reported with average moduli along with coefficient of variability in parentheses.

4.3.3 Asphalt-Bound Layer Stiffness

Stiffnesses for asphalt-bound layers are modeled by Equations (1) and (2). It is necessary to determine the model parameters required for using Equations (1) and (2).

These parameters can be determined from a set of beam frequency sweep tests in the laboratory at temperatures representing in-situ pavement conditions. Frequency sweep test data are available for the two structural asphalt-bound layers, i.e., the HMA overlay and the original HMA surface. Frequency sweep tests were conducted on beams cut from slabs of the asphalt-bound layers taken out of the pavement at the projects sites between wheelpaths. The tests were performed at three temperatures (10°C, 20°C, and 30°C), one strain level (100 microstrain), and two replicates. A summary of the density for beams used in frequency sweep tests is listed in Table 4.9. According to the table, beams from the MEF-3 site had lower air-void contents than those from the MEF-2 site.

An *Excel* workbook developed by Per Ullidtz to accompany *CalME* was used to fit the frequency sweep test data and to identify the master curve parameters. The model parameters identified are listed in Table 4.10, while the fitting of the master curves for the individual layers is shown in Figure 4.7 to Figure 4.10. Note that these model parameters are defined in Equation (1). According to Table 4.10, HMA materials from the MEF-3 site are stiffer than those from the MEF-2 site, which may be due to the lower air-void contents at MEF-3 site, as shown in Table 4.9.

In additional to using frequency sweep test data, layer moduli backcalculation using FWD data provides another method for evaluation of HMA material stiffnesses. A comparison of the stiffnesses obtained from frequency sweep (FS) and FWD tests is shown in Figure 4.11. Note that the combined HMA layer in the FWD backcalculation does not include the OGFC layer. The equivalent loading time for the FWD tests was roughly 0.015 second after the conversion to constant creep load, and this corresponds to 10 Hz for a sinusoidal load.

Pavement temperatures were calculated from the surface temperature and average air temperature of the previous day using the BELLS equation for production testing (called BELLS3 in some other publications), according to ASTM Standard D7228-06a. For the combined HMA layer, the temperature was represented at 133 mm depth. Daily average air temperatures required by the BELLS equation were determined by taking the average of the daily maximum and minimum temperatures from the OPCP weather station (see Section 4.2.1). The resulting average air temperature was 8°C for March 27, 2007 and 3.9°C for March 28, 2007.

Table 4.9: Summary of Density for Beams* Used in Frequency Sweep Tests

Mix	Rice Maximum Theoretical Specific Gravities	Air-Void Content (%)	
		Average	Standard Deviation
HMA Overlay for MEF-2	2.554	5.5	0.6
Original HMA for MEF-2	2.557	5.0	1.0
HMA Overlay for MEF-3	2.542	3.7	0.5
Original HMA for MEF-3	2.513	2.7	0.9

*: Beams were sawed out of a field slab taken from between wheelpaths.

Table 4.10: Asphalt-Bound Layer Stiffness Model Parameters Used in *CalME*

Mix	δ	E_{ref} (MPa)	β	γ	aT
MEF-2, HMA Overlay	2.30	6,266	-0.2922	0.6560	1.1232
MEF-2, Original HMA	2.30	9,108	-0.5674	0.6176	1.1005
MEF-3, HMA Overlay	2.30	8,519	-0.4107	0.7071	1.0276
MEF-3, Original HMA	2.30	15,277	-1.4151	0.7441	0.9061
FS Average, Original HMA	2.30	12,192	-0.9912	0.6809	1.0033
FS Average, HMA Overlay	2.30	7,392	-0.3515	0.6816	1.8802
FWD Average, Original HMA	2.30	7,002	-0.3515	0.6816	1.8802
ATPB or OGFC	2.30	1,185	1.6398	0.6789	0.7536

*: Reference moduli (E_{ref}) are given for loading time of 0.015 sec (i.e., loading frequency of 10 Hz); reference temperature is 20°C; and for all the mixes, A=9.6307 and VTS = -3.5047.

According to Figure 4.11, the general trends of temperature dependency are consistent for FWD stiffnesses and FS stiffnesses. FWD stiffnesses are roughly the same for the two MEF sites when pavement temperatures are the same. Further, FWD stiffnesses are lower than FS stiffnesses when temperatures are the same, even though large scatter exists for FWD stiffnesses. FWD stiffness is believed to represent actual in-situ HMA stiffness better than FS stiffness because FWD testing samples more locations along the pavement section. The large difference between FWD stiffness and FS stiffness can be attributed to two factors: (1) difference in sampling locations; and (2) difference in testing conditions.

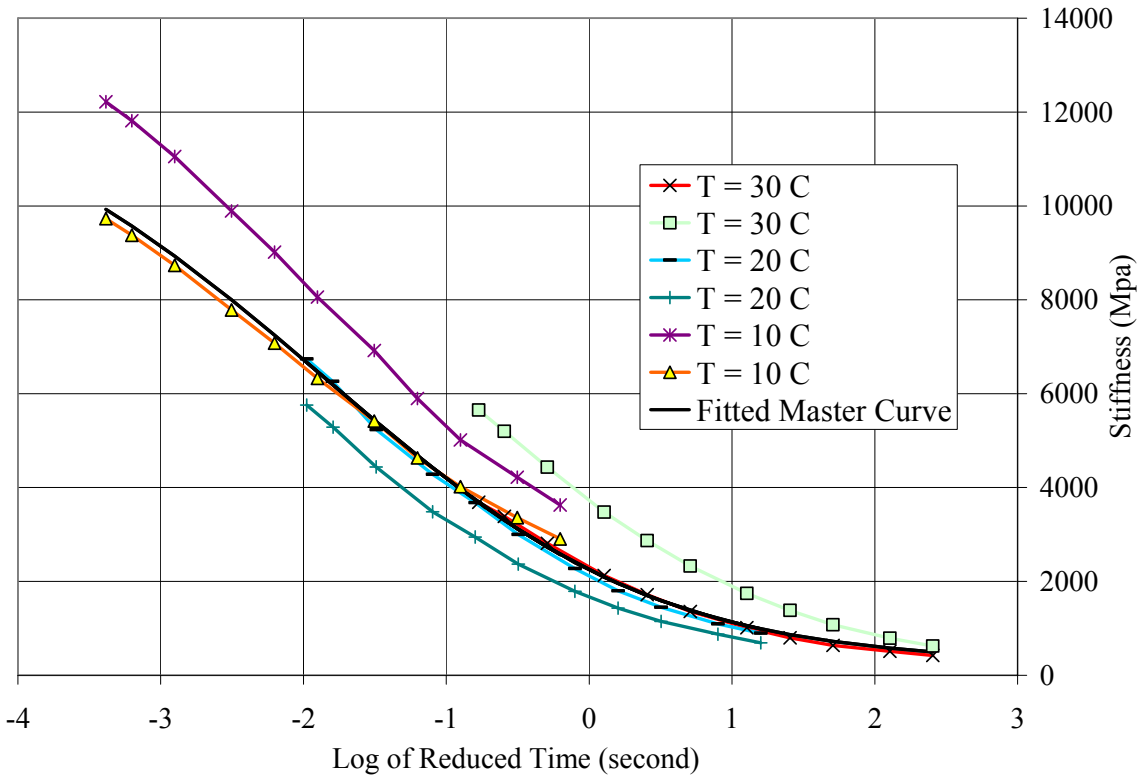

Figure 4.7: Fitting of master curve using frequency sweep data for HMA overlay at MEF-2.

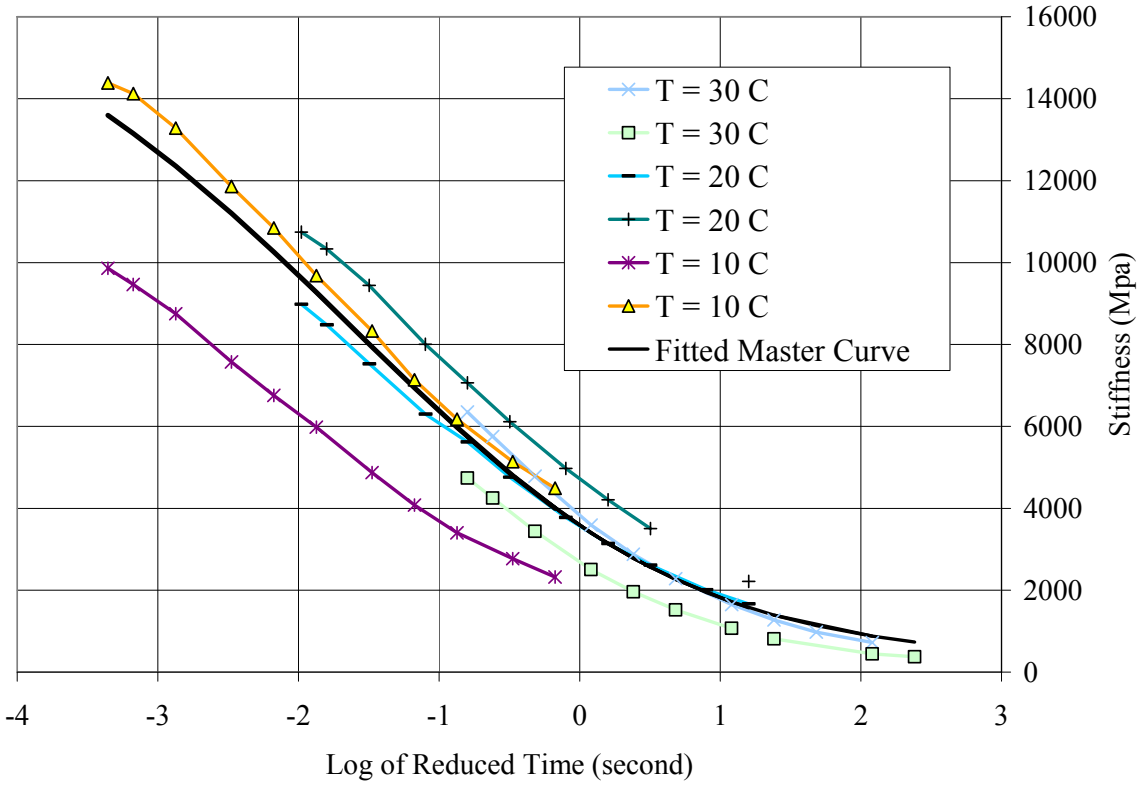

Figure 4.8: Fitting of master curve using frequency sweep data for original HMA surface at MEF-2.

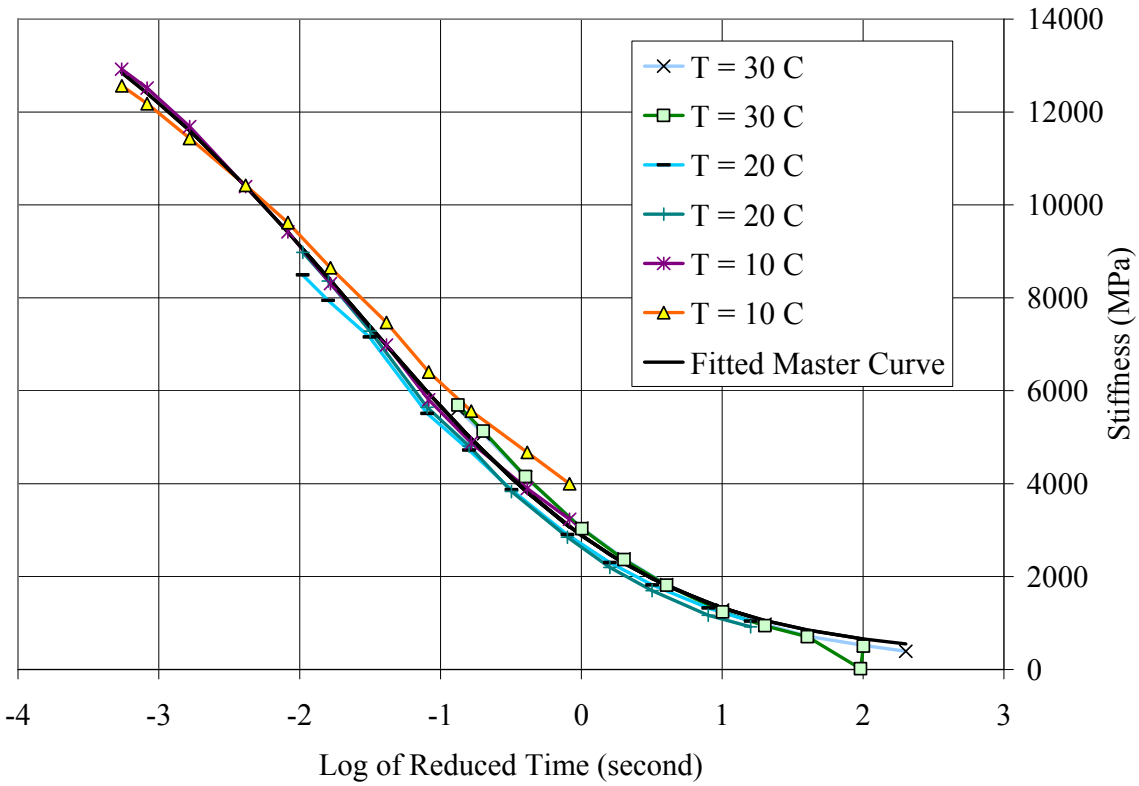

Figure 4.9: Fitting of master curve using frequency sweep data for HMA overlay at MEF-3.

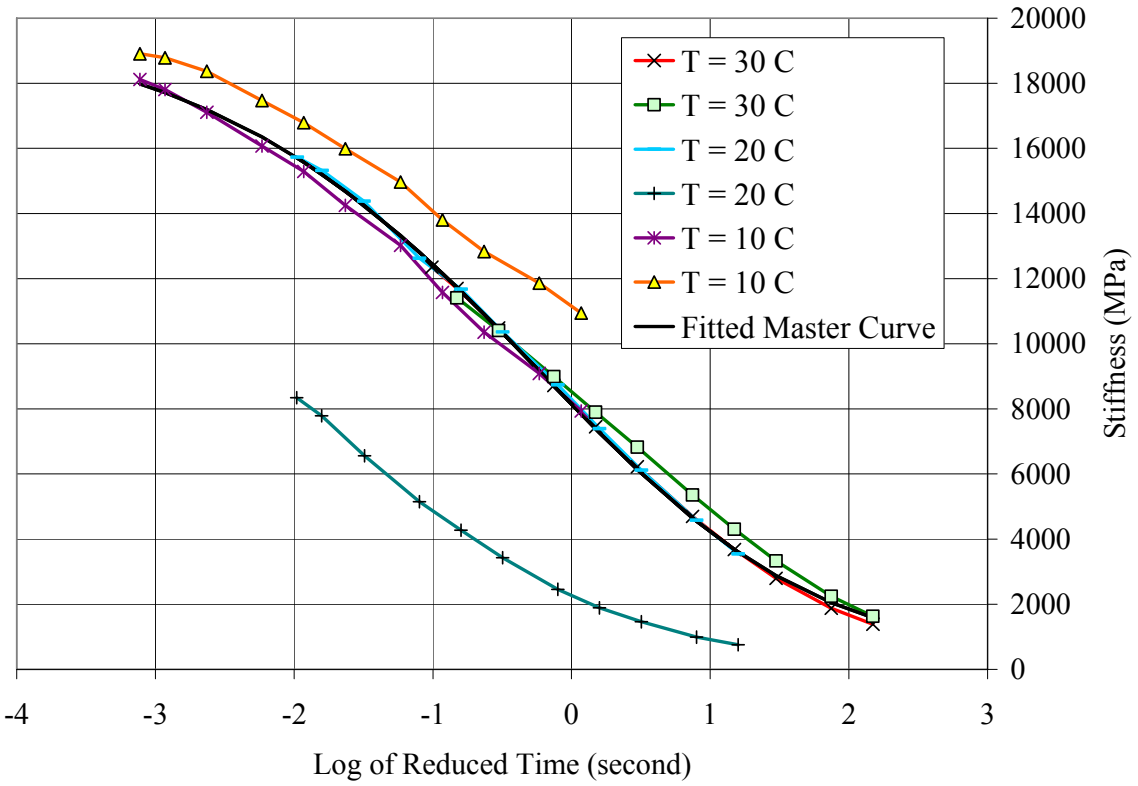

Figure 4.10: Fitting of master curve using frequency sweep data for original HMA surface at MEF-3.

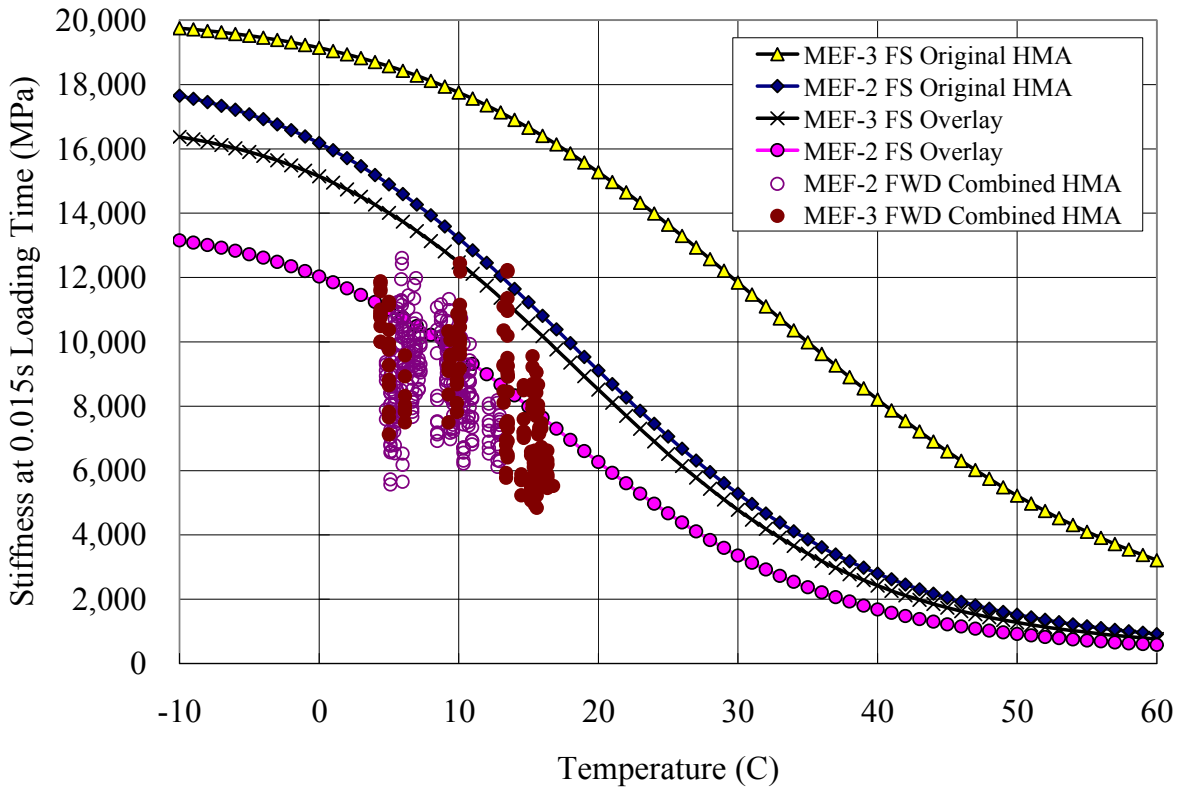

Figure 4.11: Comparison of HMA stiffnesses obtained from FS (frequency sweep) and FWD tests.

The variation of backcalculated HMA stiffnesses with pavement temperature calculated using the BELLS equation is shown in Figure 4.12, in which the values for the locations where samples were taken for FS testing are highlighted. As shown in the figure, the HMA FWD stiffnesses at the sampling location are roughly the lower bound for the MEF-2 site and roughly the upper bound for the MEF-3 site. Based on this observation, the FS stiffnesses of samples taken for the MEF-2 and MEF-3 sites roughly represent the lower and upper bounds of FS stiffness throughout the two project sites, respectively. The large difference between FWD stiffness and FS stiffness should therefore mostly be due to the different test conditions.

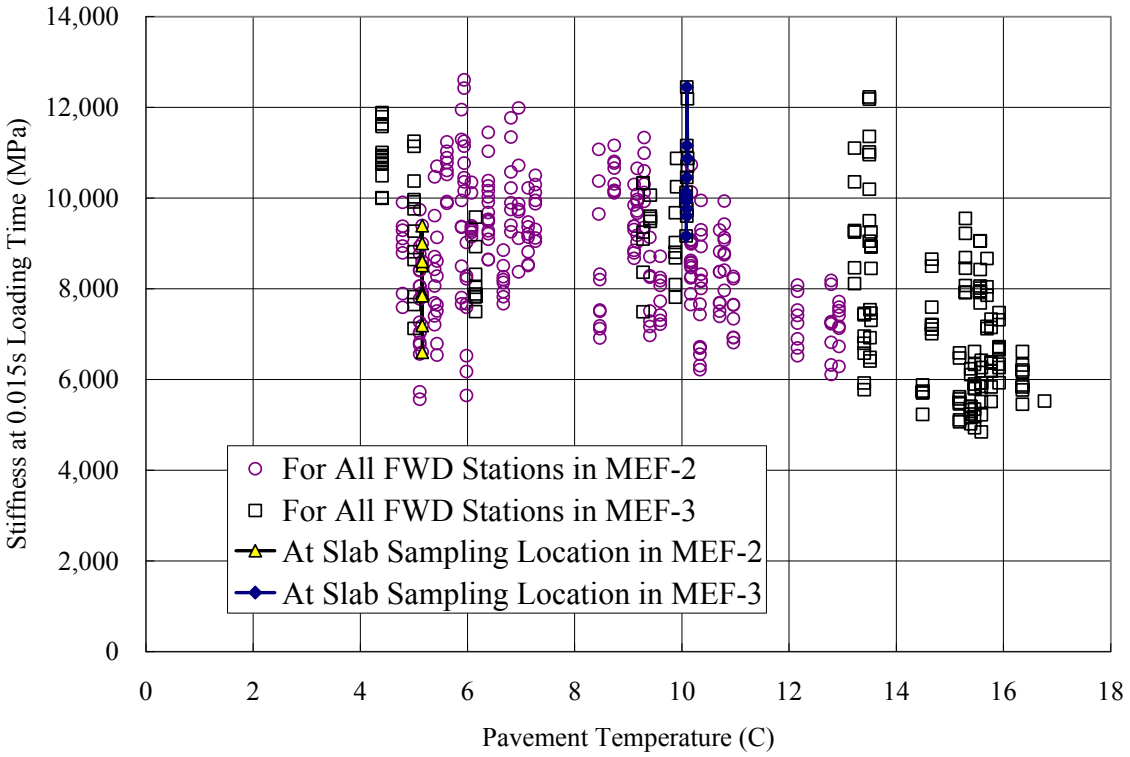

Figure 4.12: Comparison of FWD stiffnesses at different locations.

For design purposes it is important to be able to use FS stiffnesses because FWD stiffnesses are unavailable at the design stage. On the other hand, FWD stiffnesses are more representative of the actual in-situ condition because they are based on field testing data. It was therefore decided to conduct calibrations using both FWD and FS stiffnesses. Based on the fact that FWD stiffnesses are roughly the same for the two MEF sites, the same master curve was used for the two MEF sites.

The FS stiffness master curve that represents both the MEF-2 and MEF-3 sites was taken as the average of the master curves determined from samples for MEF-2 and MEF-3 individually. Specifically, this was done by taking the average of all of the master curve parameters. The average master curve parameters are listed in Table 4.10 in the row with "FS Average, Original HMA."

According to Table 4.10, the average original HMA FS stiffness at 20°C is 12,192 MPa, while the average overlay FS stiffness is 7,392 MPa. According to Figure 4.11, the average FWD stiffness for the combined HMA layer is about 6,000 MPa. To calculate the FWD stiffness for each HMA layer, it was assumed that the stiffness ratios between original HMA and overlay are the same for the FS and FWD results. Furthermore, the following equation needs to be satisfied in order to maintain the overall bending resistance of the combined layer. Equation (23) is derived from Odemark's method of equivalent thickness.

$$h_{combined}E_{combined}^{1/3} = h_{original}E_{original}^{1/3} + h_{overlay}E_{overlay}^{1/3} \quad \textbf{(23)}$$

where E is layer stiffness,
h is layer thickness

The resulting FWD stiffness at 20°C is 7,002 MPa for the original HMA and 4,271 MPa for the overlay. The closest match for 7,002 MPa in Table 4.10 was the reference FS stiffness for the overlay (7,392 MPa). Accordingly, the master curve for the FWD stiffness of the original HMA was assumed to be the same as the one for the average overlay FS stiffness, except that the E_{ref} was changed to 7,002 MPa

Since frequency sweep tests and FWD testing were conducted on materials that had been placed in the field for 10 years before being overlaid, it was necessary to account for aging. The original HMA surface was placed using AR4000 binder. The effects of aging on stiffness for HMA mixes with AR4000 binder were reported by Harvey and Tsai *(8)*. According to this research *(8)*, it is very important to identify the source of the binder between coastal and valley sources because mixes with coastal binder are softer and more susceptible to aging, while mixes with valley binder are stiffer and less susceptible to aging. The reference moduli are around 2,200 MPa for virgin coastal mixes and 8,300 MPa for virgin valley mixes. After six days of long-term oven aging (LTOA), the reference moduli increased to around 4,200 MPa (a 91 percent increase) for coastal mixes and 11,000 MPa (a 33 percent increase) for valley mixes.

Generally, six days of LTOA corresponds to 8 to 18 years of aging in the field, depending on the climate *(9)*. Considering the relatively cool climate at the two project sites, six-day LTOA was assumed to represent 15 years of aging in the field and three-day LTOA to correspond to 7.5 years of aging in the field.

Based on the reference moduli of the HMA materials taken from the field for the two projects, it was believed that the AR4000 mixes used in the two projects had binder from sources similar to valley sources.

The stiffness increase caused by aging for the original HMA surface should be less than 33 percent but higher than 22 percent due to the decreasing rate of aging over time. It was assumed that the stiffness for the materials taken out of the field had increased by 25 percent since construction.

The overlay material had been subjected to five years of aging. For valley mixes, three-day LTOA (i.e., 7.5 years of field aging) led to a stiffness increase of 17 percent *(8)*. It was assumed that stiffness of the overlay HMA had increased by 10 percent since 2002, the year of construction.

The material stiffness parameters for the two HMA layers, as listed in Table 4.10, needed to be adjusted to account for the aging. This was done in the following manner: by decreasing the reference moduli and δ defined in Equation (1) based on the estimated amount of stiffness increase. The adjusted reference moduli are listed in Table 4.11, and the master curves are shown in Figure 4.13.

Table 4.11: Asphalt-Bound Layer Stiffness Model Parameters After Accounting for Aging

Mix	δ	E_{ref} (MPa)	β	γ	aT
FS Average, HMA Overlay	2.26	5,914*	-0.3515	0.6816	1.8802
FS Average, Original HMA	2.20	9,754*	-0.9912	0.6809	1.0033
FWD Average, Original HMA	2.20	5,602*	-0.3515	0.6816	1.8802

*: The reference stiffness is given for 20°C and 0.015 loading time.

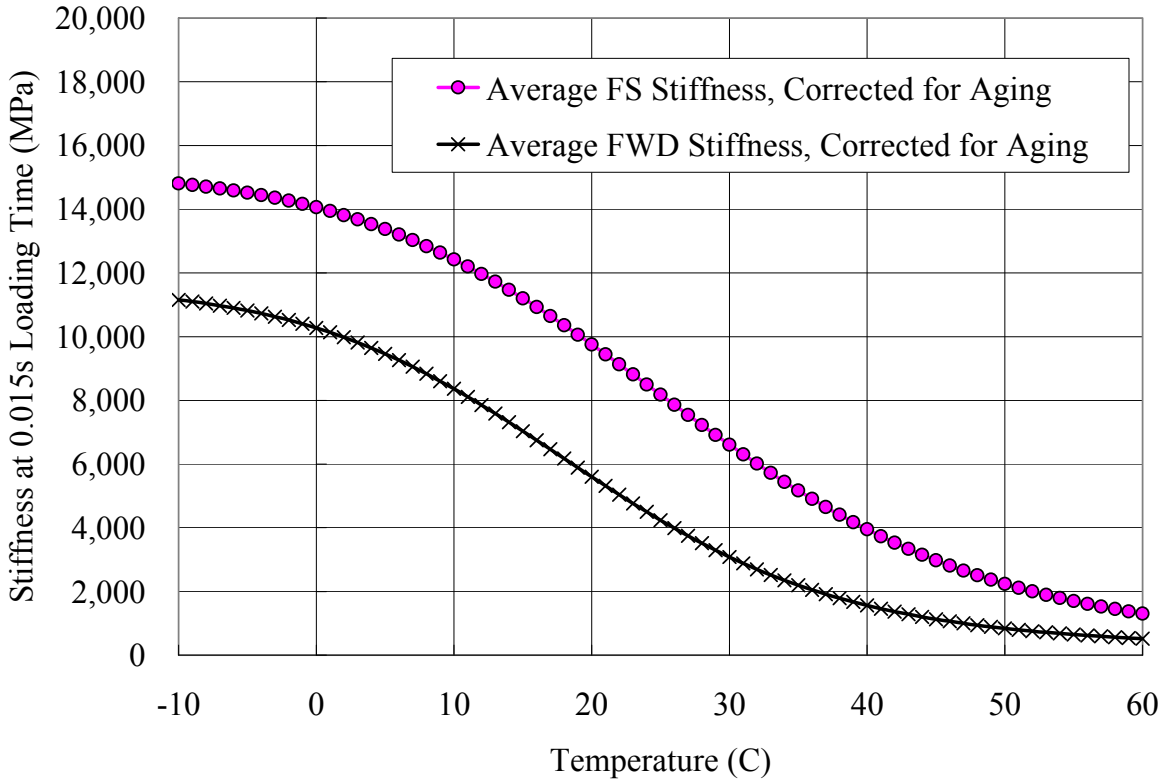

Figure 4.13: Master curves for original HMA after correction for aging.

The aging parameters as defined in Equation (4) can be determined by using the assumption that stiffness increases 25 percent over 10 years due to aging. Assuming B = 1.0, the aging parameter A can be solved to be A = 0.0305. The resulting stiffness increase over time is shown in Figure 4.14. Note that five years of aging will lead to a 23 percent increase in stiffness, which is higher than the value (i.e., 10 percent) chosen for the HMA overlay to account for the effect of aging on FS stiffness. This indicates that the aging model used may be overpredicting the stiffness increase for the location. A sensitivity analysis was conducted to evaluate the effect of aging (see Section 6.4 for more details).

The layer moduli for ATPB and OGFC were determined based on research results presented by Moore *(10)*. Specifically, moduli for ATPB and OGFC were assumed to be the same, and the master curve should provide the best fit for the following resilient modulus (AASHTO T274-82) results shown in Table 4.12.

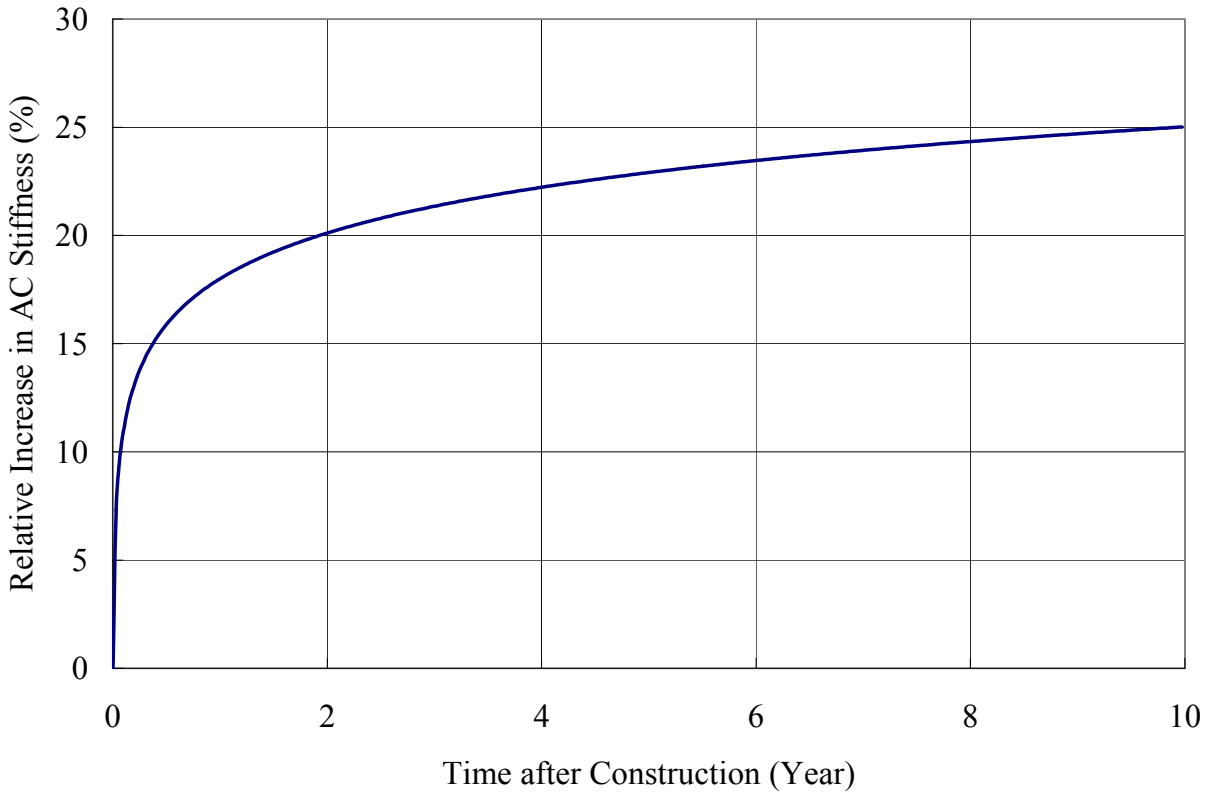

Figure 4.14: Relative increase in HMA stiffness over time.

Table 4.12: Measured ATPB and OGFC Resilient Modulus Reported in Reference *(10)*

Temperature	Resilient Modulus (ksi)	Resilient Modulus (MPa)
4.4°C/40°F	522	3,599
21.1°C/70°F	141	972
21.1°C/70°F	157	1,082
22.2°C/72°F	159	1,096
23.9°C/75°C	155	1,069
32.2°C/90°F	70	483

These measured values are consistent with tests results reported in Reference *(11)*. Note that the resilient modulus was measured using a haversine waveform with a 0.1-sec loading time and 0.9-sec rest period. The loading frequency is hence on the order of 10 Hz. The *Excel* workbook for frequency sweep test data was used to fit a master curve through the measured values listed in Table 4.12. The fitted stiffness model parameters are listed in Table 4.10. For soaked conditions, the stiffnesses need to be reduced by half according to Reference *(11)*. Based on descriptions of the cores taken from the field, the ATPB layer did not come out as an intact layer. It is believed that the ATPB layer had been soaked and damaged, and therefore soaked stiffness should be used. This was also verified by the FWD backcalculation.

In layer moduli backcalculation as well as in *CalME* simulation, the ATPB and OGFC layers were both assumed to be linear elastic unbound materials rather than asphalt-bound materials. For ATPB, this is because it is located below 140 mm depth and does not undergo large temperature variation. For OGFC, this is because it is only 25 mm in thickness and the stiffness is too low to have much structural significance. Based on FWD data backcalculation results, the actual layer moduli used was 3,000 MPa for OGFC and 500 MPa for ATPB.

The low stiffness for ATPB indicates its degradation. Once ATPB is damaged, it is believed to act similarly to AB layers, and therefore its stiffness depends on the confinement from the layers above. The parameters for the confinement effect for ATPB are the same as the ones used for the AB layer, which is described in Section 4.3.4. Accordingly, it was decided to combine the ATPB and AB layer into one layer in the *CalME* simulations.

4.3.4 Unbound Layer Stiffness Model Parameters

Unbound materials, including aggregate base and subgrade, were treated as linear elastic materials with stiffness a function of the confinement provided by the over-burden layers. The in-situ stiffnesses were backcalculated using deflection data from FWD tests conducted both along the centerline and between the wheelpaths (see Table 4.6 and Table 4.8). The assumption is that there was very little traffic-induced damage in the unbound layers, and that the stiffness degradation was caused by the weakening of confinement.

The model parameters defined in Equation (20) were identified by fitting the backcalculated unbound layer stiffness. The variation of backcalculated AB stiffness with confinement and FWD drop load are shown in Figure 4.15 and Figure 4.16 respectively when SG was assumed to be linear. Figure 4.17 and Figure 4.18 show the same plots, but for cases where SG was assumed to be nonlinear. Apparently, the confinement and load level effects on AB stiffness are much more pronounced when SG is treated as nonlinear material. Since SG is actually treated as nonlinear material in *CalME*, the unbound layer stiffnesses were determined from FWD backcalculation results obtained with the nonlinear SG assumption.

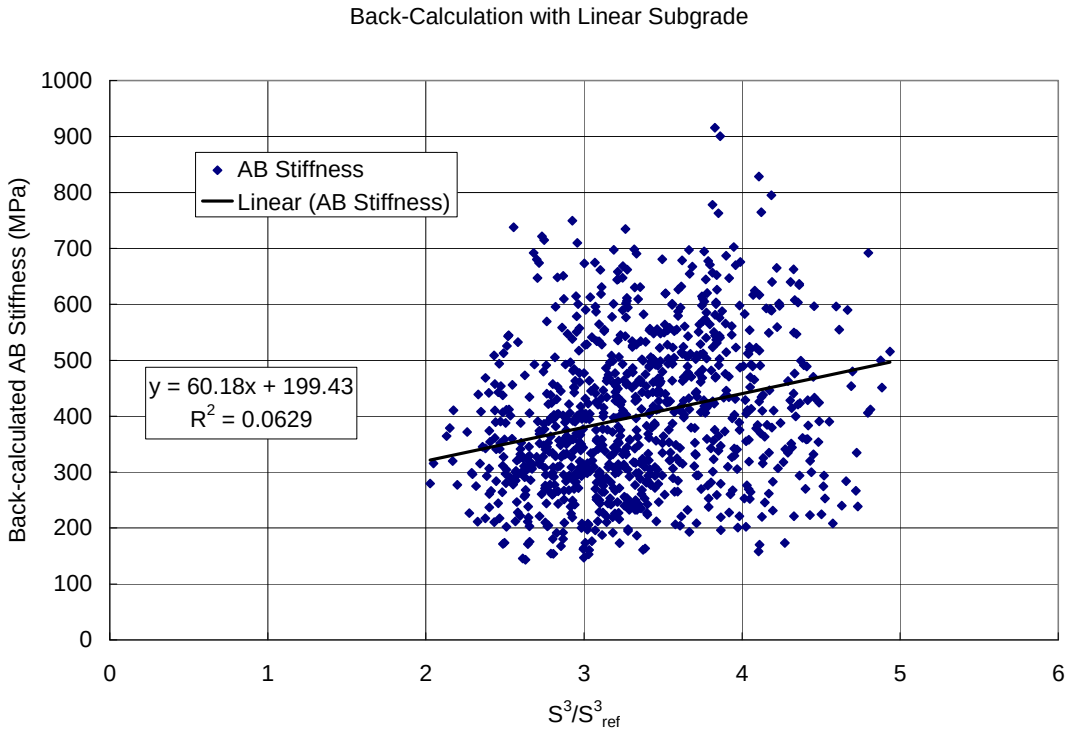

Figure 4.15: Lack of strong correlation is shown by variation of backcalculated AB stiffness with confinement when SG is assumed to be linear.

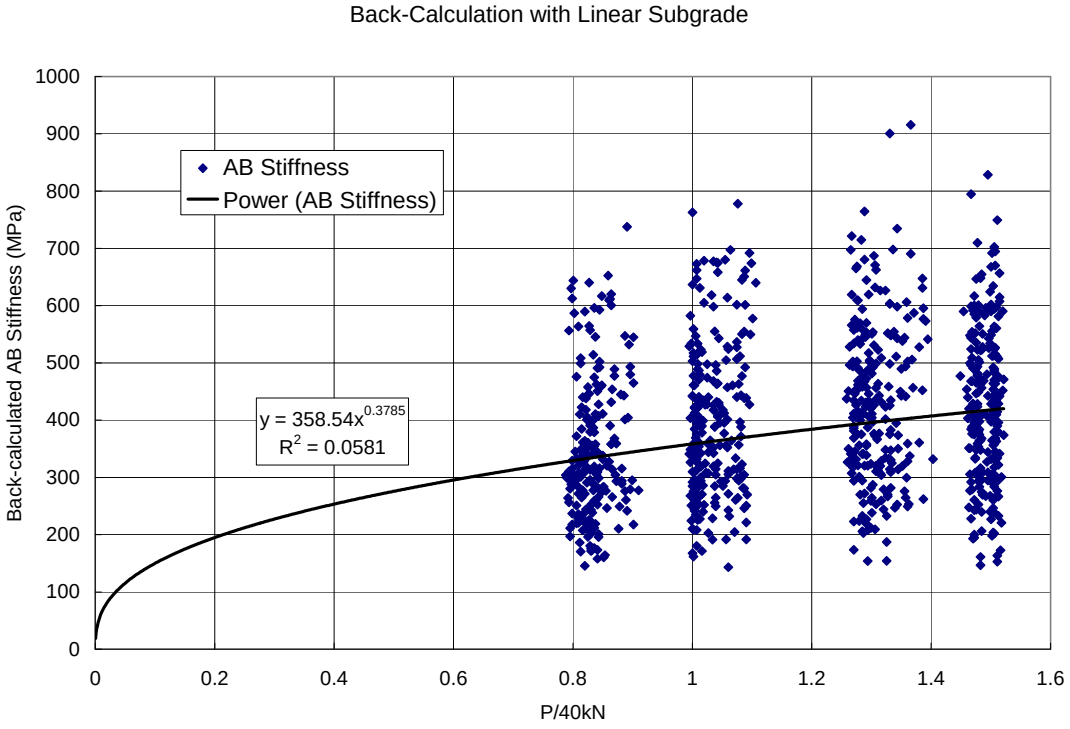

Figure 4.16: Lack of strong correlation is shown by variation of backcalculated AB stiffness with FWD drop load when SG is assumed to be linear.

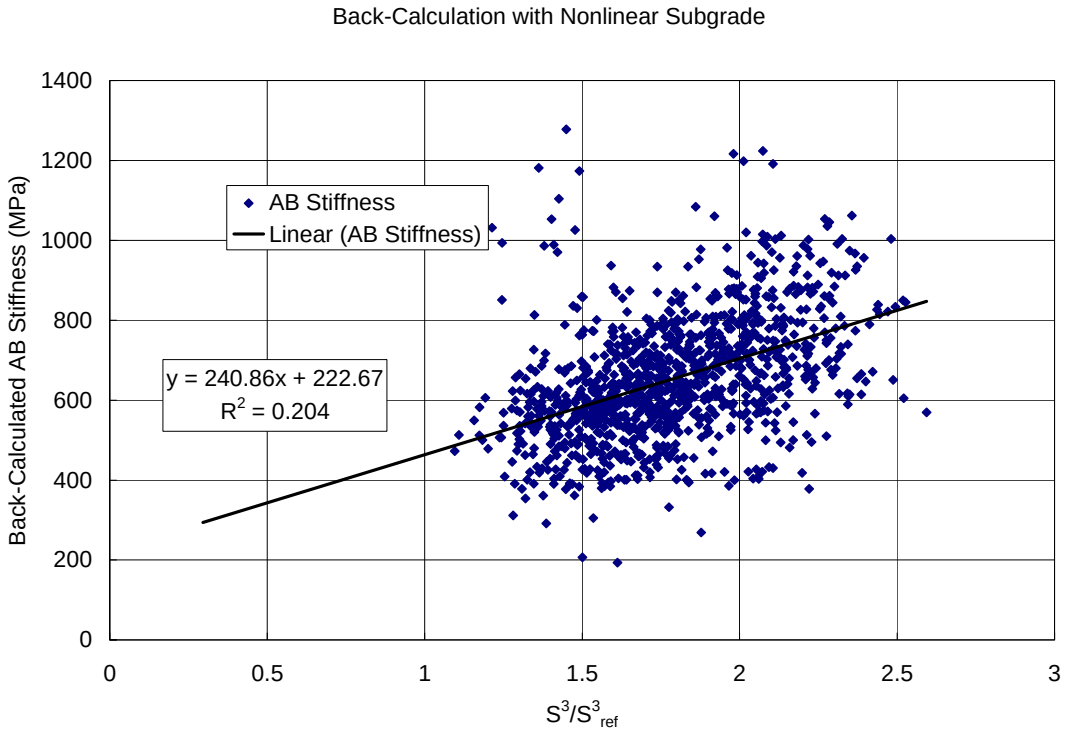

Figure 4.17: Variation of backcalculated AB stiffness with confinement when SG is assumed to be nonlinear; compared to when SG is assumed to be linear (as in Figure 4.15), this figure shows relatively strong correlation.

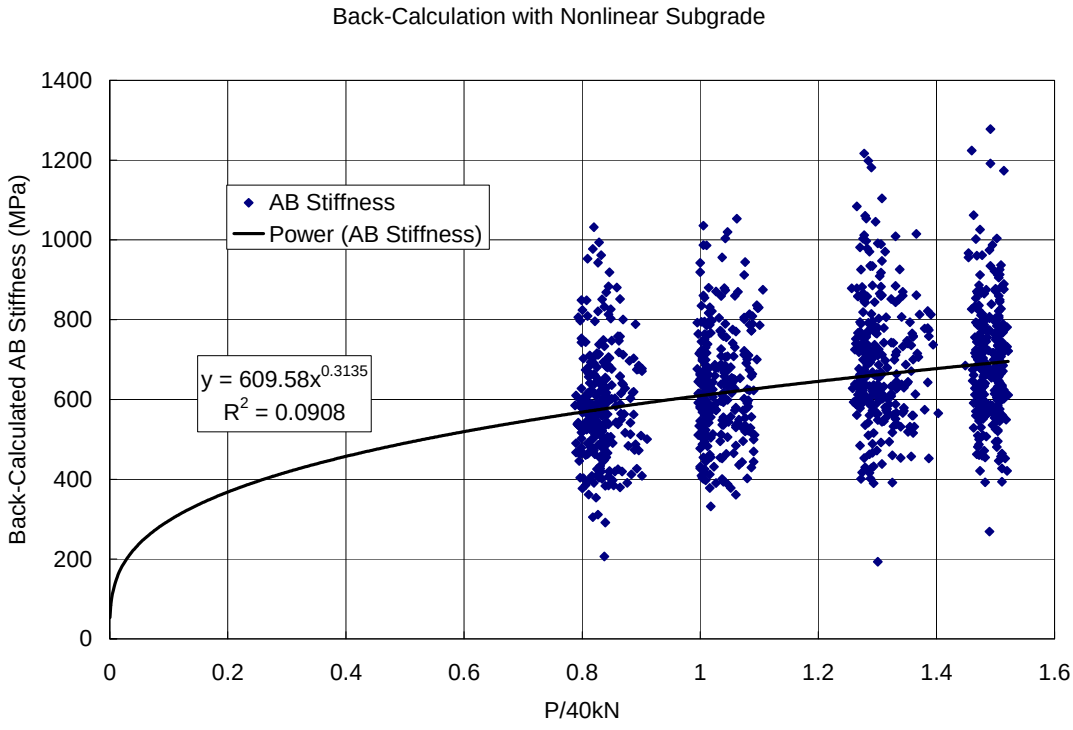

Figure 4.18: Variation of backcalculated AB stiffness with FWD drop load when SG is assumed to be nonlinear; compared to when SG is assumed to be linear (as in Figure 4.16), this figure shows relatively strong correlation.

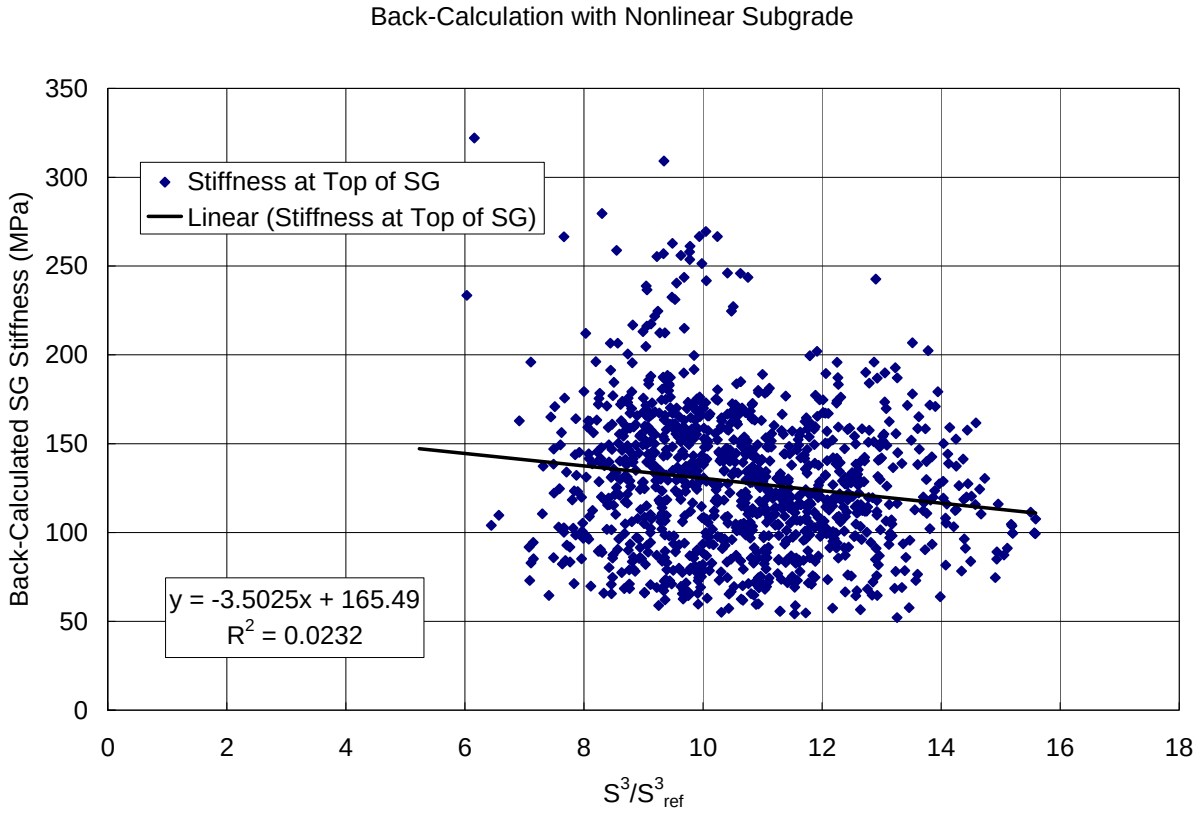

Figure 4.19: Lack of correlation is shown by variation of stiffness at the top of the SG layer with confinement effect, assuming nonlinear SG.

The effect of confinement on stiffness at the top of the SG layer is shown in Figure 4.19, which indicates that there is no evidence at all of a strong effect of confinement. Accordingly no confinement effect was considered for the SG layer. This suggests that *StiffnessFactor* for SG is 0.

AB stiffness model parameters were identified by fitting backcalculated AB stiffness with Equation (20). According to Table 4.8, AB stiffnesses are roughly the same for the two MEF sections, thus only one set of model parameters was identified. SG stiffness model parameters were identified by fitting backcalculated top of SG stiffness with Equation (17). Since *StiffnessFactor* is zero, the reference stiffness of SG is equal to the average backcalculated FWD stiffness. The nonlinear factor α was equal to the average of the backcalculated nonlinear factor *n*. The reference stiffnesses for the AB layers were calculated and are listed in Table 4.13, along with those for the SG layers.

The unbound layer stiffness model parameters used for calibration of the WesTrack project are listed in Table 4.14. According to the table, the values obtained here for *StiffnessFactor* and α are all consistent.

Table 4.13: Unbound Layer Stiffness Model Parameters

Material	E_{ref} (MPa)	*StiffnessFactor*	α
AB in both	474	0.44	0.17
SG in MEF-2	105	0.0 (ignored)	-0.36
SG in MEF-3	150	0.0 (ignored)	-0.28

Table 4.14: Unbound Layer Stiffness Model Parameters for WesTrack Materials

Description	S_{ref} (mm·MPa$^{1/3}$)	*StiffnessFactor*	α
ATPB + Aggregate Base (AB)	3500	0 ~ 0.65	0.6
Subgrade (SG)	3500	0	-0.2

In *CalME*, the stiffness entered for an unbound layer is not E_{ref}, rather it is the stiffness that matches the reference stiffness of the HMA layers on top of it under 40 kN loading. Accordingly, the input values for the AB layer stiffness needs to be calculated using Equation (17). The calculated AB layer stiffnesses to be entered in *CalME* are listed in Table 4.15. As indicated in the table, AB stiffnesses for the two MEF projects are practically the same. It was therefore decided to use average AB stiffness for both projects, depending on the type of HMA stiffness used.

Table 4.15: Calculation of *CalME* Model Parameters for AB Layer

Material	Original HMA Stiffness Type	Original HMA Thickness (mm)	Original HMA Stiffness (MPa)	S (mm·MPa$^{1/3}$)	AB Stiffness (MPa)
AB in MEF-2	FWD Stiffness	138	7,135	2,657	357
AB in MEF-2	FS Stiffness	138	11,125	3,081	408
AB in MEF-3	FWD Stiffness	140	7,135	2,695	361
AB in MEF-3	FS Stiffness	140	11,125	3,125	414
AB in Both	FWD Stiffness	-	-	-	359
AB in Both	FS Stiffness	-	-	-	411
SG in MEF-2	All stiffness	-	-	-	105
SG in MEF-3	All stiffness	-	-	-	150

Note that the ATPB layer was combined with the AB layer in *CalME,* and the material properties for AB were used for the combined layer.

4.3.5 Rutting Model Parameters for Asphalt-Bound Material

Rutting model parameters for the two structural asphalt-bound layers (i.e., the HMA overlay and the original HMA surface) were determined using data from RSST-CH tests conducted by UCPRC for a similar HMA mix used for the PPRC Strategic Plan Element 4.10 project *(5)*. This was done by minimizing the root mean square error between predicted and measured inelastic strain in the RSST-CH tests. The inelastic strain model is shown in Equation (7). The RSST-CH test data are stored in a comprehensive database maintained by the UCPRC database manager. An *Excel* workbook was developed by Per Ullidtz using the "Solver" function to both import the shear test data and to perform the minimization.

For PPRC SPE 4.10, eighteen RSST-CH tests were conducted for each experimental mixture, with two levels of temperature (45°C and 55°C), three levels of stress (70, 100 and 130 kPa) and three replicates. The reference shear stress τ_{ref} was set to 0.1 MPa (the default value in *CalME*). To compare the fitted permanent shear strain with the measured ones, a normalized permanent shear strain $\gamma^{i}_{normalized}$ defined below was used:

$$\gamma^{i}_{normalized} = \ln\left(\gamma^{i} \Big/ \exp\left(\beta \times \tau \Big/ \tau_{ref} \right) \times \gamma^{e} \right) \qquad \textbf{(24)}$$

in which the variables are the same as defined in Equation (7). A comparison of calculated and measured normalized permanent shear strain for different surface HMA mixes is given in Figure 4.20. The shift factor *K* is set to 1.4 based on HVS calibration *(1)*.

Table 4.16: HMA Mixes Rutting Model Parameters for Use in *CalME*

Type	A	α	τ_{ref} (MPa)	β	γ	K*
"g" (gamma)	0.805	2.60	0.1	0.349	2.91	1.4

*: K is the shift factor that needs to be adjusted as part of the calibration process so that the calculated rut can match the measured values.

Rutting model parameters for the ATPB layer were taken to be the same as those for the aggregate base, which are listed in Table 4.17. This is because the ATPB layer was assumed to behave similarly to the aggregate base, given the extensive damage in the layer observed from cores.

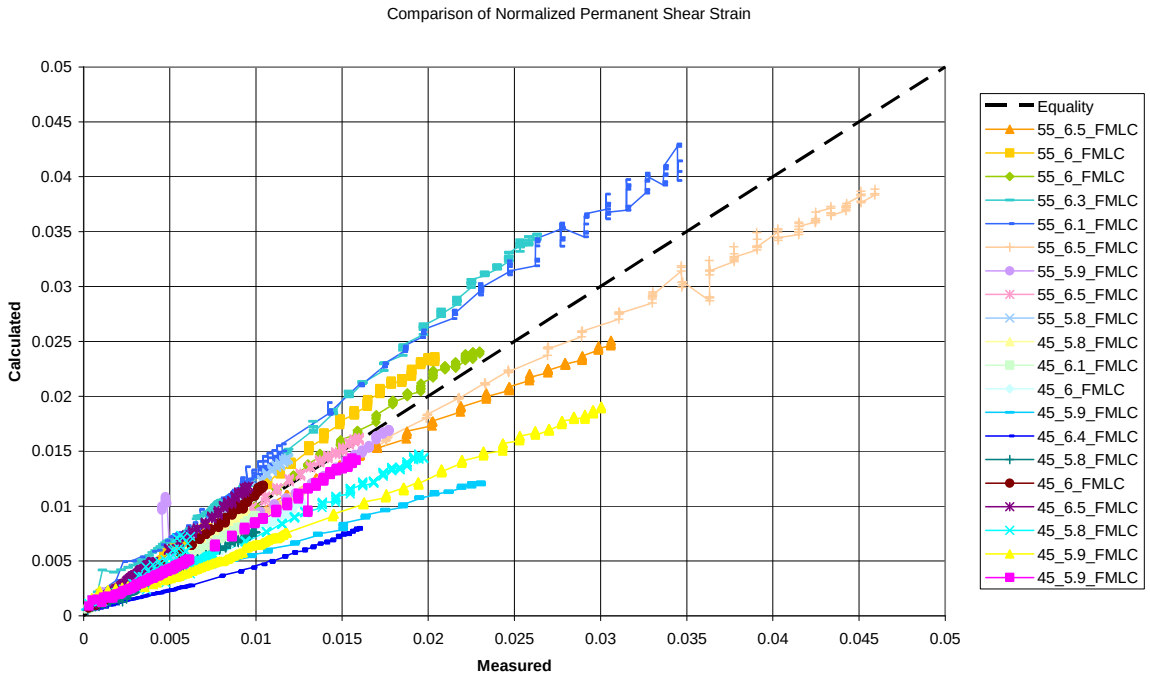

Figure 4.20: Comparison of fitted and measured normalized permanent shear strain from RSST-CH test results for HMA mix used in Goal 9 Project.
(Note: The legend indicates testing temperature (°C) and air-void content, along with specimen preparation method; FMLC means the specimen was prepared by compaction in the lab using loose mix taken from the field.)

4.3.6 Rutting Model Parameters for Unbound Layers

The rutting model parameters for the aggregate base and subgrade were taken from the default *CalME* materials library for materials named "AB" and "SC." The actual values are listed in Table 4.17. These are generic rutting model parameters that are the same for all aggregate bases and clayey sands, respectively.

Table 4.17: Unbound Material Rutting Model Parameters for Use in *CalME*

Mix	Type	A	α	ε_{ref} (ue)	β	E_{ref} (MPa)	γ
Aggregate Base	"e"	0.8	0.333	1000	1.333	40	0.333
Subgrade	"e"	3.5	1.0	578	4.48	160	0.0

4.3.7 Fatigue Model Parameters for Asphalt-Bound Material

Asphalt-bound materials include the OGFC and ATPB layers, as well as the HMA overlay and the original HMA surface. Both OGFC and ATPB are assumed to accumulate no fatigue damage. For OGFC this is because of its small thickness and because it does not perform as a structural layer. For ATPB, this is because the large air voids in the material and microcracks are assumed to have no effect on its structural capacity.

For the two HMA layers, fatigue parameters can be determined by fitting the bending beam fatigue test data. Beams were cut from slabs of the asphalt layer (see e.g., Figure 4.22) taken from the highway between

wheelpaths. Fatigue tests were conducted at three temperatures (10, 20 and 30°C), two strain levels (200 and 400 microstrain), and with three replicates. When the beam fatigue testing results were fit, data points with a residual stiffness ratio below 0.30 were ignored because that data typically does not accurately reflect how the beams behave, as they have been severely cracked. Measured theoretical maximum specific gravities and air-void contents for the specimens are listed in Table 4.18. The fatigue parameters are listed in Table 4.19. A comparison of observed laboratory fatigue life, defined as the number of repetitions required to reach 50 percent stiffness reduction in fatigue tests, is shown in Table 4.20. According to the table, the original HMA for MEF-2 had better laboratory fatigue performance than the one for MEF-3 at 20°C and 30°C, but it had worse performance at 10°C. A comparison of the average stiffness reduction curves for materials taken from the two sites is shown in Figure 4.21.

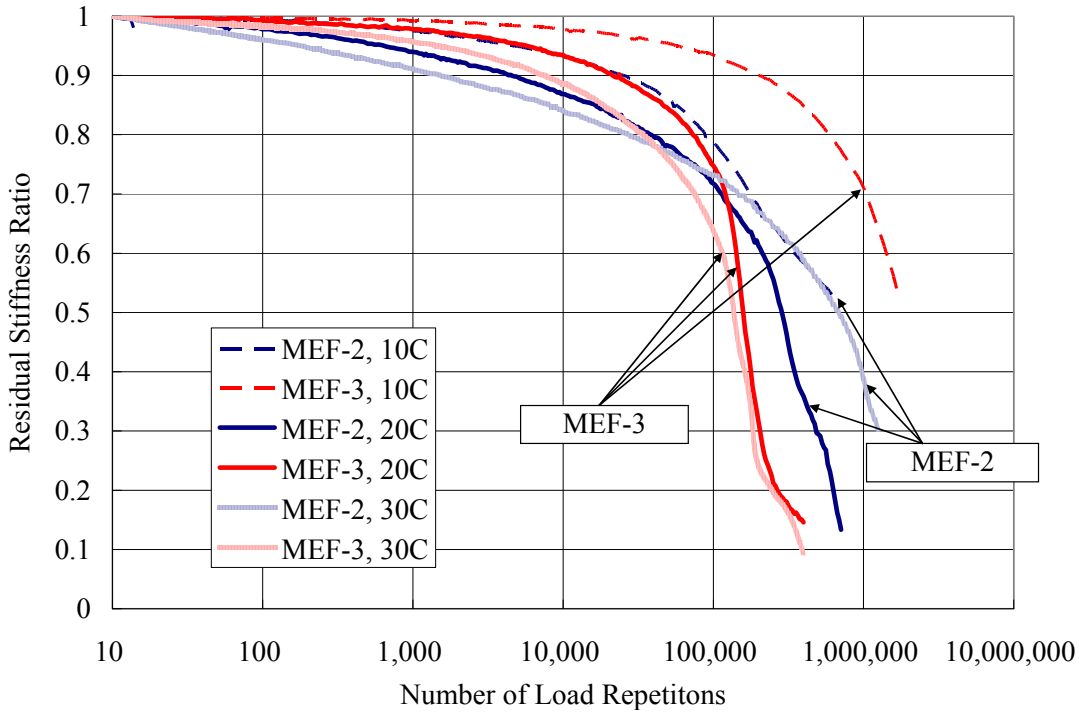

Figure 4.21: Comparison of stiffness reduction curves for original HMA materials sampled from MEF-2 and MEF-3 sites tested with 200 microstrain.

Based on FWD backcalculation results (Section 4.3.3), the FS stiffness determined from HMA materials sampled from a single location in the field should not be used to represent the whole pavement section. Instead, average FS stiffness was used to represent HMA stiffness for both MEF-2 and MEF-3. A similar approach was used to develop fatigue model parameters to represent both MEF-2 and MEF-3. Specifically, fatigue model parameters were determined by fitting fatigue test data for both MEF-2 and MEF-3. The resulting model parameters are listed in Table 4.19 in the row "Original HMA for Both."

Table 4.18: Summary of Density for Beams Used in Fatigue Tests

Mix	Rice Maximum Theoretical Specific Gravities	Air-Void Content (%)	
		Average	Standard Deviation
Original HMA for MEF-2	2.557	5.1	0.8
Original HMA for MEF-3	2.513	2.4	1.2

Table 4.19: HMA Layer Fatigue Model Parameters for Use in *CalME* (i.e., Equations [9] to [11])

Mix	Type*	A	α_0	ε_{ref} (με)	β	E_{ref} (MPa)	γ	δ
Original HMA for MEF-2	"u"	64.55	-0.830	200	-1.89	3000	-0.945	0
Original HMA for MEF-3	"u"	9598	-0.833	200	-6.63	3000	-3.31	0
Original HMA for Both	"u"	171.1	-0.842	200	-2.96	3000	-1.48	0

*: Type "u" indicates unified fatigue model described in Equations (9) to (11).

Table 4.20: Comparison of Fatigue Life for HMA Mixes Under 200 Microstrain (millions of repetitions)

Mix	10°C	20°C	30°C
Original HMA for MEF-2	1.205	0.344	0.876
Original HMA for MEF-3	2.303	0.191	0.173

Figure 4.22: Cutting slabs of HMA layers from the pavement between wheelpaths.

4.3.8 Construction Variability

In *CalME*, construction variability is needed to conduct Monte Carlo simulation. Random variables considered in Monte Carlo simulation include the following quantities:

1. Layer thickness, normal distribution;
2. Layer stiffness, log-normal distribution; and
3. HMA layer model parameters: *A* for both fatigue [i.e., defined in Equation (11)] and rutting [i.e., defined in Equation (7)], both follow log-normal distribution.

The mean values for these random variables have already been discussed. What remains is the variability of these quantities. *CalME* provides default values. With the available data, variations were determined for HMA layer thickness, and AB and SG stiffness (specifically, the top of the SG layer) as listed in Table 4.21; *CalME* default values were used for all the other quantities.

Table 4.21: Construction Variability Determined with Available Data

Quantity	Coefficient of Variation or Standard Deviation Factor	Data Source
HMA Thickness	0.05	Slab thickness
AB Stiffness	1.23	FWD backcalculation
SG Stiffness	1.30	FWD backcalculation

4.4 Traffic

CalME provides a database of load spectra based on WIM (Weigh-In-Motion) data collected throughout the state. The closest WIM station near the project sites is WIM020, which is installed near Loleta, California, on US 101 near postmile 65.6 in Humboldt County. The load spectrum for the project site was assumed to be the same as that for WIM020 although it is on the other side of the nearest city, Eureka.

The truck traffic volume was extracted from the Annual Average Daily Traffic (AADT) data provided by Caltrans through the website, *http://www.dot.ca.gov/hq/traffops/saferesr/trafdata/*. According to the traffic data, the traffic volume at the project sites was roughly one quarter of the volume recorded for WIM020. For *CalME* simulation, only the truck traffic is needed. The Annual Average Daily Truck Traffic (AADTT) counts along with regression fitting are shown in Figure 4.23. The AADTT counts were fitted using the following equation:

$$AADTT(year) = 430 \times (1 + 0.02)^{year - 1992} \quad \textbf{(25)}$$

Note that AADTT actually decreased in 1993 compared to 1992. This can be explained by the separation of through traffic and around traffic for the nearby Redwood National Park starting in mid-1992. The AADTT data for years after (including) 1993 is believed to more closely match the actual traffic for the project site in 1992.

Equation (25) indicates that the base AADTT for *CalME* simulation is 430 since the original pavement structure opened to traffic in 1992. The axle per year per design lane can be calculated using the following equation:

$$AxlePerYearPerDesignLane = AADTT \times 365 \times f_{dir} \times f_{lane} \times AxlesPerTruck \quad \textbf{(26)}$$

where: f_{dir} is the directional distribution factor,
f_{lane} is the lane factor.

According to Reference *(12)*, the traffic pattern at WIM station number 020 can be classified into Group 1a, which has an average lane factor of 0.87 and varies between 0.53 and 0.97. Using a lane factor of 0.87 for the truck lane of a four-lane highway, a directional distribution factor of 0.5, and an *AxlesPerTruck* value of 3.40 for WIM station WIM020, the axles per year per design lane for the beginning year 1992 was calculated to be 232,127.

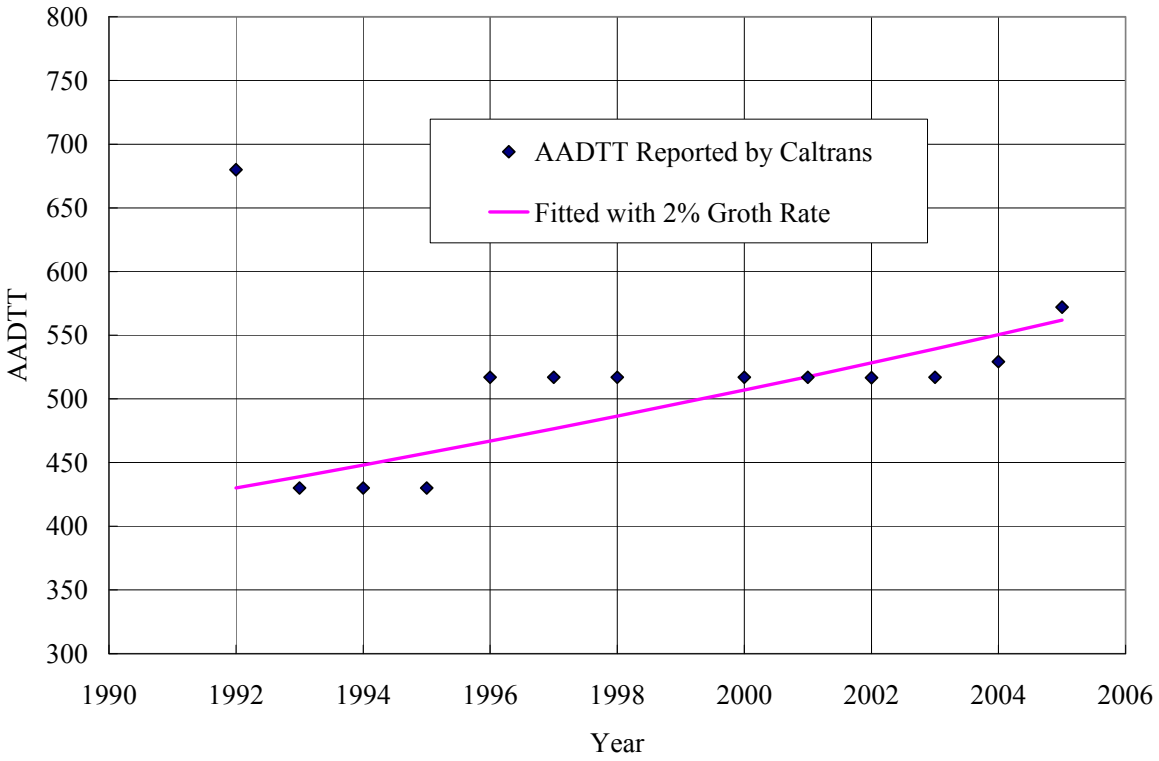

Figure 4.23: Regression of annual average daily truck traffic count (AADTT), with a base AADTT of 430 in 1992 and a growth rate of two percent.

CalME outputs ESAL counts in simulation results, which allows one to calculate the ratio between axle count and ESAL count. For the two MEF sites, one passage of a typical axle is on average equivalent to 0.315 ESALs. This is determined by the traffic load spectra for WIM020. The traffic volume for the two MEF sites is then 73,120 ESALs for the first year (i.e., 1992), which increased at a rate of 2 percent per year.

CalME also takes into account the speed of the truck traffic. The default value in *CalME* is 70 km/hour (43 mph). A study based on WIM data collected throughout California *(12)* indicates that highway traffic speed has an average value of roughly 91 km/hour (57 mph) and a standard deviation of roughly 10 km/hour (6.2 mph). The actual traffic speed at the project sites depends on the traffic volume and the longitudinal profile of the highway.

According to the Caltrans AADT database, AADT was roughly 4,200 from 1992 to 2005. This implies roughly one vehicle passing every 45 seconds, which indicates relatively light traffic at the project sites. Elevation variations along US 101 near the two MEF sites are shown in Figure 4.24, which were obtained by using *Google Earth* software. Note that *Google Earth* uses SRTM 90 m digital elevation data *(http://srtm.csi.cgiar.org),* whose vertical error is reported to be less than 16 m. The figure shows that both MEF-2 and MEF-3 are located on a climbing section with an overall slope of roughly 7 percent. Therefore, the truck speeds are expected to be slower than on flat pavement sections.

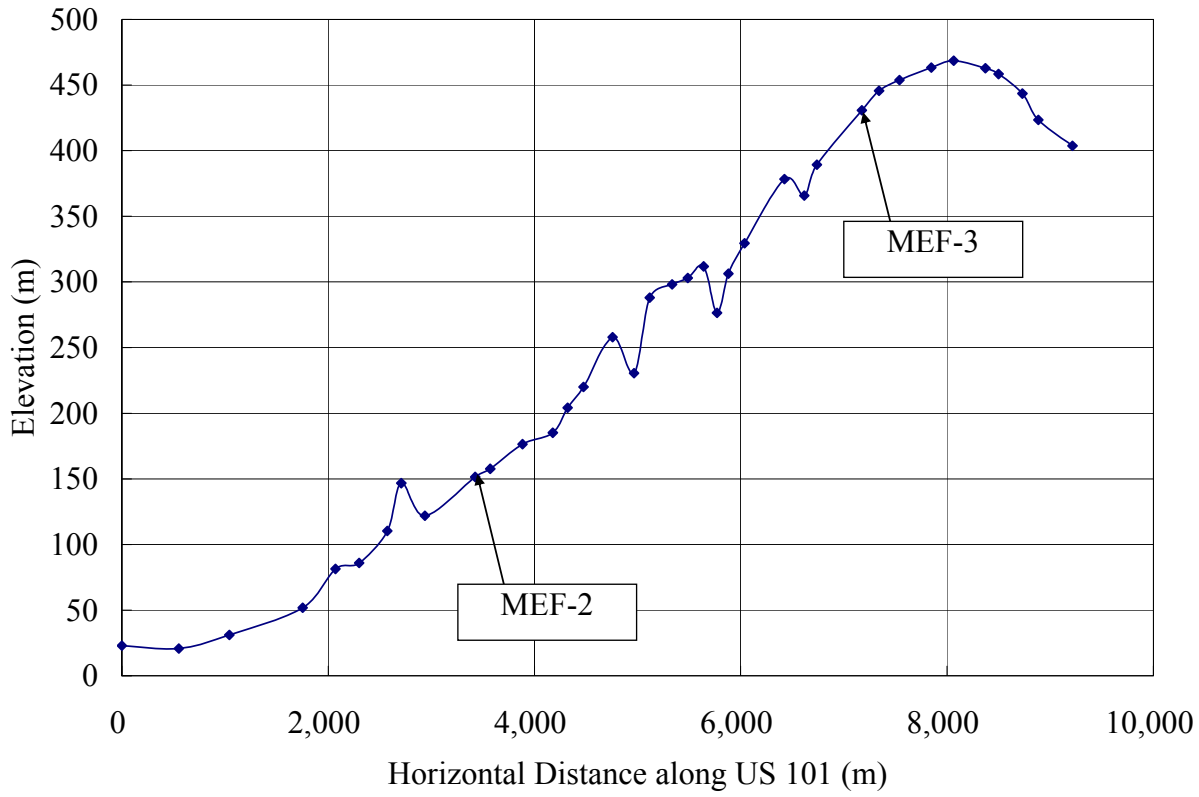

Figure 4.24: Elevation variation along US 101 near the project sites.

A portable WIM station was used to measure the actual highway truck speed and weight on the northbound truck lane at the MEF-2 site (i.e., postmile 127.5) from 15:53 hours on April 7, 2008 to 20:36 hours on April 8, 2008. A total of 253 trucks were recorded for the period and the truck speed histogram is shown in Figure 4.25. According to the figure, a bimodal distribution can be identified for the truck speed. Slower trucks traveled at

speeds between 30 to 37.5 mph, while faster trucks traveled at speeds between 50 to 62.5 mph. The portable WIM data also indicate that heavier trucks tend to travel at slower speeds. Based on these observations, traffic speed was set to be 35 mph (56 km/hr), which is weighted towards the heavier, more damaging trucks. Traffic speeds for the two MEF sites were assumed to be the same based on their close proximity and the similar terrain. A sensitivity study was conducted to evaluate the effects of traffic speed on fatigue cracking performance (see Section 6.5 for more details).

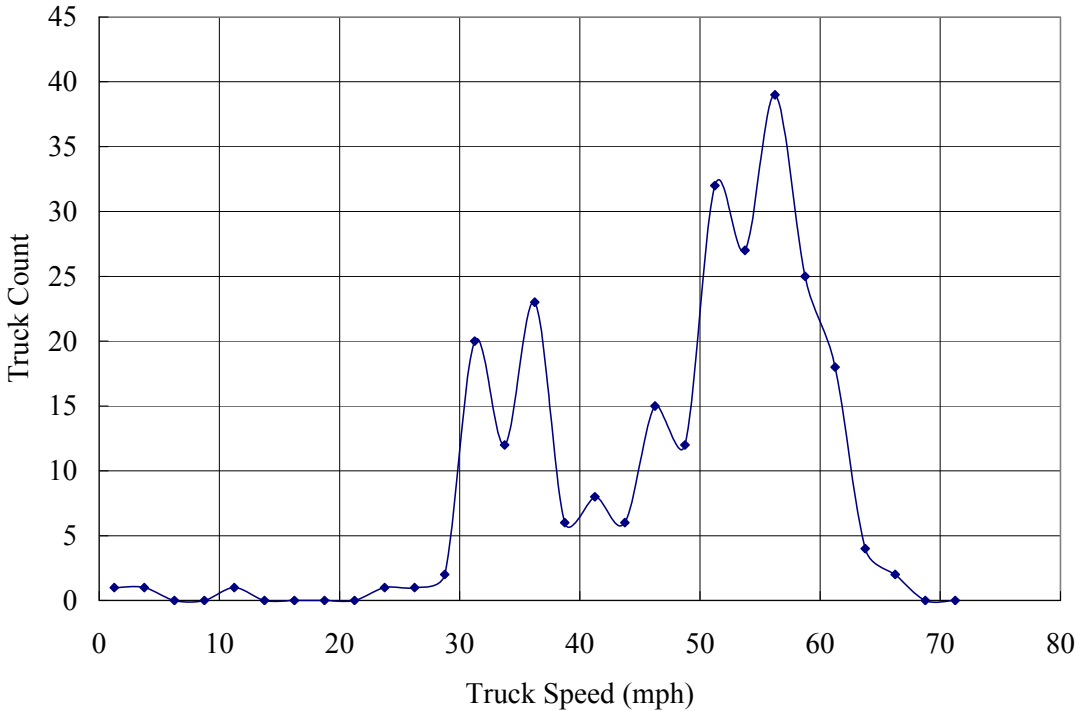

Figure 4.25: Truck speed histogram measured at the beginning of MEF-2 (PM 127.5).

4.5 Performance

Cracking performance measurements of the pavement segments at the two project sites were extracted from the Pavement Condition Survey (PCS) data in the Caltrans PMS database. The segments used for data extraction were 1.0-mile long, centered at the project locations listed in Table 2.1. The pavement condition survey segments that overlap with the project pavement segments are shown in Figure 4.26 for MEF-2 and Figure 4.27 for MEF-3. In these figures, the pavement segments of interest are indicated with a thick solid line for each year (red if shown in color); the PCS survey segments that are overlapping are plotted with thin lines indicating the beginning and ending postmiles. For example, Figure 4.27 shows that there was only one survey done overlapping the MEF-3 project range in year 2002 and the survey started from PM 128.8 and ended at PM 130.7. Data from different dynamic segments in the PCS data were combined using the algorithm described in Reference *(13)*.

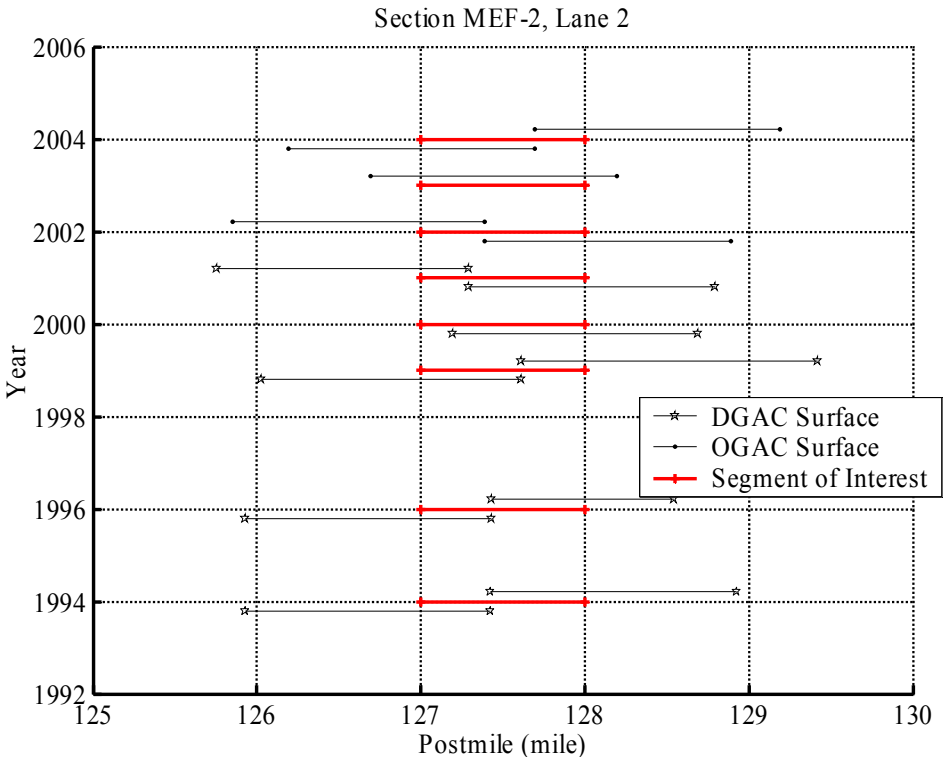

Figure 4.26: Survey data segments available for project site MEF-2, northbound lane 2.

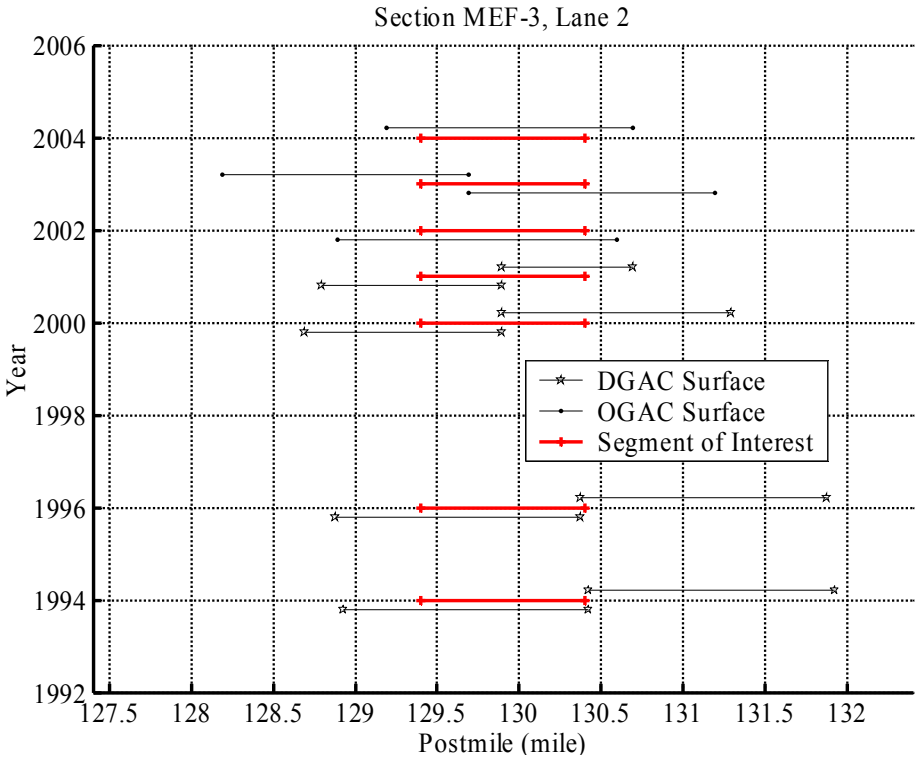

Figure 4.27: Survey data segments available for project site MEF-3, northbound lane 2.

The extracted distresses include both type A and type B alligator cracking. The sum of both type A and B alligator cracking is the total wheelpath cracking, which is plotted in Figure 4.28. As shown in the figure, cracks started to show up on the surface in 1999 for MEF-2 and in 2000 for MEF-3. The decrease in crack density in 2001 compared to 2000 coincides with the change of surface type from DGAC to OGAC, indicating some maintenance occurred in year 2001. This suggests that the crack density data after (including) year 2001 should be discarded when comparing calculated performances with observed ones. No surface cracking appeared after the original pavement was overlaid in 2002. The opening date for the original pavement was assumed to be August 1, 1992.

Using a failure criterion of 10 percent wheelpath cracking, the fatigue cracking life for MEF-2 is about 8 years, while the fatigue cracking life for MEF-3 is between 8 to 9 years and is taken as 8.5 years for calibration purposes. Based on the traffic data shown in Section 4.4, the truck lane at MEF-2 has experienced 0.63 million ESALs, while MEF-3 has experienced 0.67 million ESALs. According to the district materials engineer, both pavement sections were designed for 10 years with a traffic index (TI) of 9.5 (1.27 to 1.98 million ESALs) using an R-value of 15. Apparently the pavements failed roughly two years before their design life ended, and with approximately 33 to 55 percent of their design traffic. Although no specific reason for the failures was identified, this kind of premature failure is not uncommon given the variability in construction and the expected variability in service life for pavements designed using the empirical method.

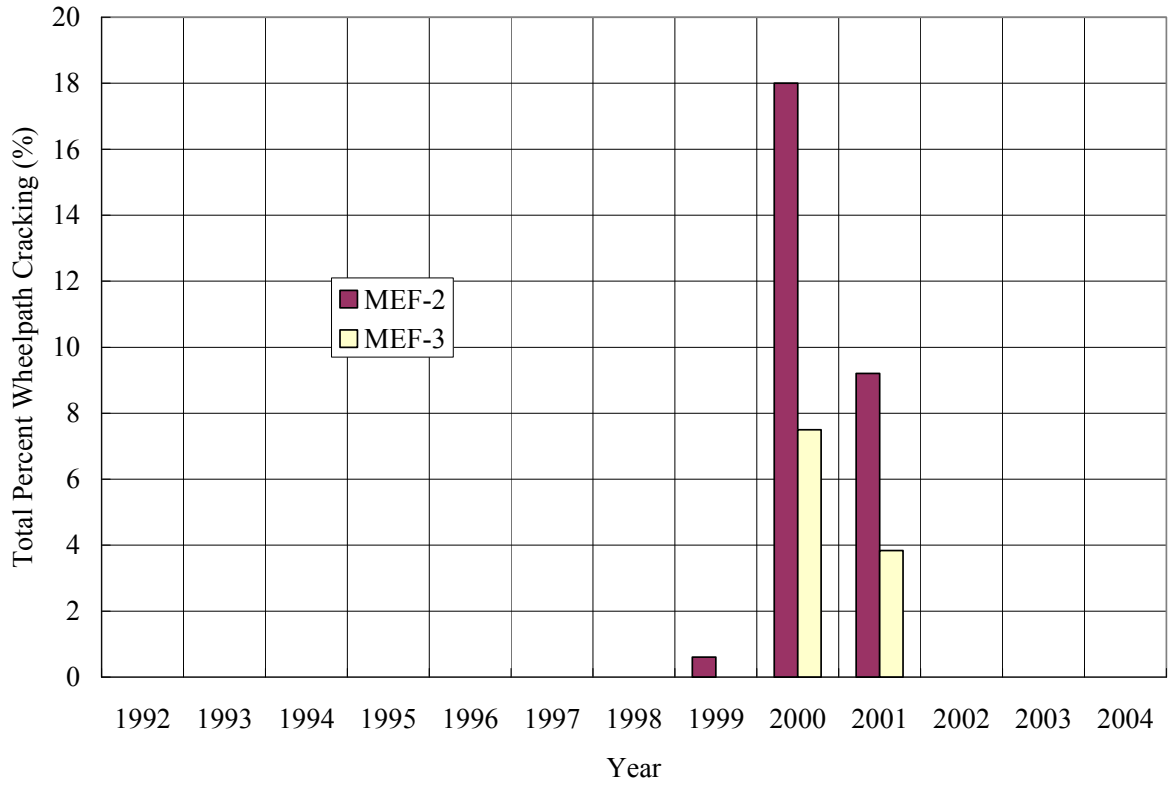

Figure 4.28. Total percent wheelpath cracking for the two sites.

4.6 Comparison of Model Inputs for the Two Projects

Based on the results presented in this chapter, the two projects share a number of common model inputs. A comparison of model inputs for the two projects appears in Table 4.22, which shows that the two projects are only slightly different in terms of layer thicknesses, AB and SG stiffness, and wheelpath cracking history.

Table 4.22: Comparison of Model Inputs for the Two Projects

Input Category	Model Input	Comparison between MEF-2 and MEF-3
Environment	Temperature	Same
Structure	Layer thickness	Slightly different
Structure	HMA stiffness	Same
Structure	AB stiffnesses	Same
Structure	SG stiffnesses	Different
Structure	HMA fatigue parameters	Same
Structure	HMA rutting parameters	Same
Traffic	Traffic volume	Same
Traffic	Traffic speed	Same
Performance	Wheelpath cracking history	Slightly different

5 *CALME* OPERATION

This chapter describes some of the key details for running *CalME* and for performing model calibration. Note that these discussions may become obsolete with future versions of *CalME*.

5.1 Mode of *CalME* Analysis

CalME can be run in various modes that determine how the user specifies model inputs and performance data. *CalME* stores data related to pavement simulation in a Microsoft *Access* database referred to as the "project database." The mode in which the program runs is determined by the value of the "HVS" field in the "ProjectLayer" table in the project database. A "0" for all layers indicates routine pavement design, a "1" indicates HVS tests, and a "2" or any other larger number indicates track tests (e.g., NCAT Test Track, WesTrack).

For calibration of *CalME* using field data, one needs to run *CalME* in routine pavement design mode. This is the default running mode so the user does not need to change the "HVS" field in the "ProjectLayer" table.

5.2 Parameters to be Calibrated

The parameter that can be adjusted to match calculated surface cracking density with measured values is the fatigue shift factor for the original HMA surface. This parameter converts the number of load repetitions in bending beam fatigue tests to the number of wheel passes in the field. The damage rate decreases with the increase in the fatigue shift factor. In other words, surface cracking develops more slowly when the fatigue shift factor increases. In particular, this shift factor can be set at the Recursive tab in the Material Property editing window.

6 RESULTS AND DISCUSSION

6.1 Introduction

This chapter presents the results obtained in the calibration study, including the sensitivity of the fatigue shift factor for the original HMA surface layer; the effects of traffic wander, HMA aging, traffic speed, and traffic volume; the sensitivity of construction variability; and the determination of fatigue shift factors for both deterministic and probabilistic analysis. A comparison of measured and calculated rutting performance is also included.

In the sensitivity studies listed below, inputs for project MEF-2 were always used. The simulations assumed no wander in order to make the simulations run faster, and the *LEAP* option was checked as the strain calculation engine. The sensitivity of pavement performance to different factors should be the same regardless of whether the traffic has or does not have wander. Sensitivity analyses used average FS (frequency sweep) stiffnesses.

The actual calibration simulations included cases with and without wander. Separate fatigue shift factors were developed for the two wander settings and the two HMA layer stiffnesses (i.e., FS stiffness and FWD stiffness).

Cracking performance of the pavement structure is represented by the *fatigue cracking life,* which is defined as the time required to reach 10 percent wheelpath cracking for all of the sensitivity analyses. The fatigue shift factor was developed for both *deterministic analysis* and *probabilistic analysis* (i.e., Monte Carlo simulation) in *CalME*.

6.2 Sensitivity of the Fatigue Shift Factor for the Original HMA Surface Layer

In order to effectively estimate the fatigue shift factor (FSF) that can provide the best fit between calculated and measured cracking performance, it is necessary to know how the simulated pavement cracking performance changes with the fatigue shift factor.

The FSF for the original HMA surface was varied between 0.025 and 0.50. The actual values used include: 0.025, 0.05, 0.1, 0.25, and 0.5. The relation between fatigue cracking life and the fatigue shift factor is shown in Figure 6.1. According to this figure, the fatigue cracking life is roughly in proportion to the fatigue shift factor. However, Figure 6.2 indicates that the traffic volume required to reach failure is exactly in proportion to the fatigue shift factor, which is expected based on the *CalME* models. The nonlinearity shown in Figure 6.1 is attributed to the nonlinear traffic growth.

Figure 6.1 indicates that an FSF of about 0.08 is needed to allow the calculated fatigue cracking life to match the actual life of eight years observed in the field for MEF-2. Accordingly, the FSF was set to 0.08 in the following sensitivity analyses unless stated otherwise. Note however, the FSF needs to be smaller than 0.08 if wander is allowed.

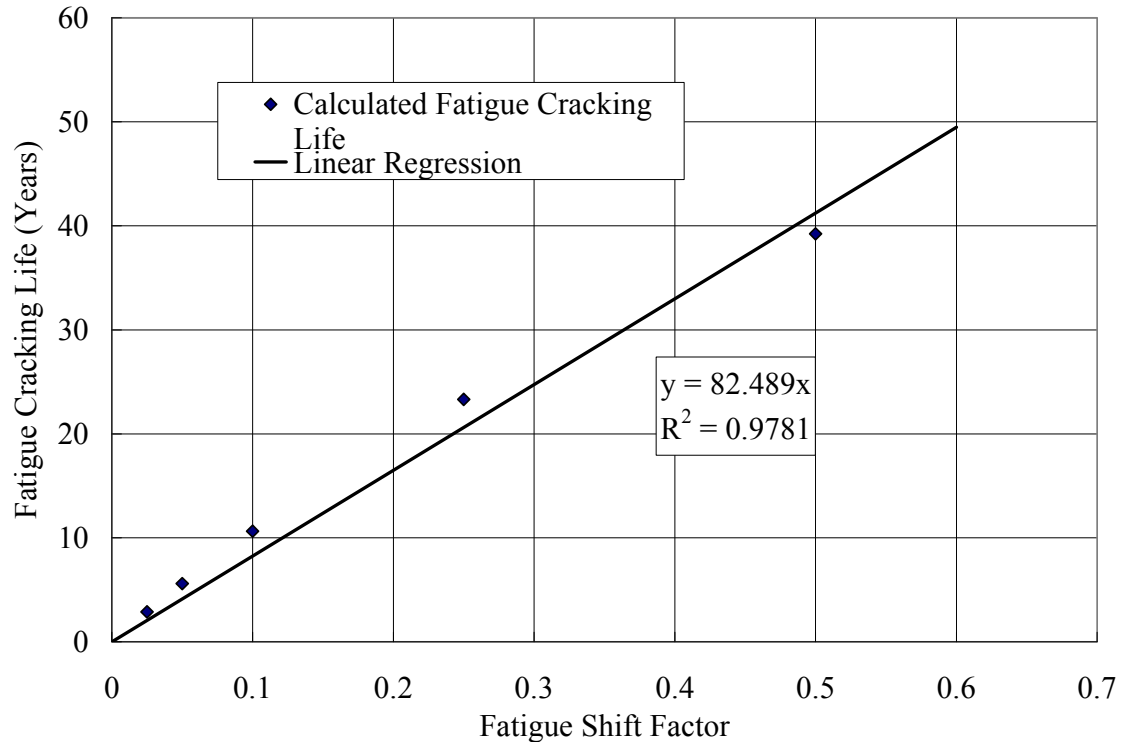

Figure 6.1: Variation of fatigue cracking life in terms of years with fatigue shift factor for the original HMA surface layer.

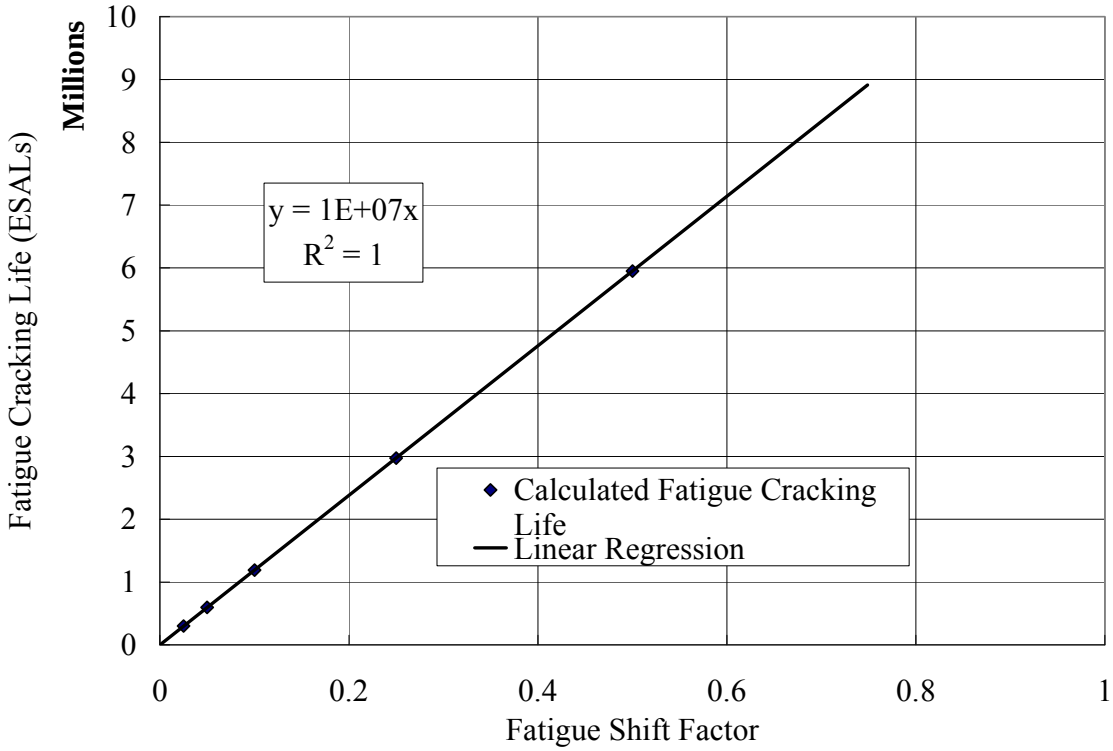

Figure 6.2: Variation of fatigue cracking life in terms of ESALs with fatigue shift factor for the original HMA surface layer.

6.3 Effect of Traffic Wander

CalME has a default wander pattern with a normal distribution for wheel positions and a standard deviation of 300 mm for transverse wheel offsets. *CalME* simulations were run with four wander settings: (1) no wander; (2) the default wander pattern in *CalME*; (3) wander with 200 mm of standard deviation in the transverse wheel position and (4) wander with 400 mm for standard deviation. The resulting surface crack development plots are shown in Figure 6.3, which demonstrates that cracking develops significantly faster when there is no wander in the traffic compared when there is wander. According to the figure, the fatigue cracking lives are 8.7, 12.1, 14.4, and 16.8 years respectively for the cases without wander, with 200 mm wander, with 300 mm wander (the *CalME* default setting) and with 400 mm wander. The fatigue cracking life is 70 percent longer with default *CalME* wander compared to the fatigue life calculated without wander.

It is believed that actual highway traffic wander has a standard deviation of between 200 and 400 mm for the transverse wheel locations. In fact, a study *(14)* shows that the standard deviation is around 307 mm. Since different FSF are determined for simulations with and without wander, using a "no wander" option will not lead to additional error while using a "with wander" option leads to potential error of 17 percent in cracking life.

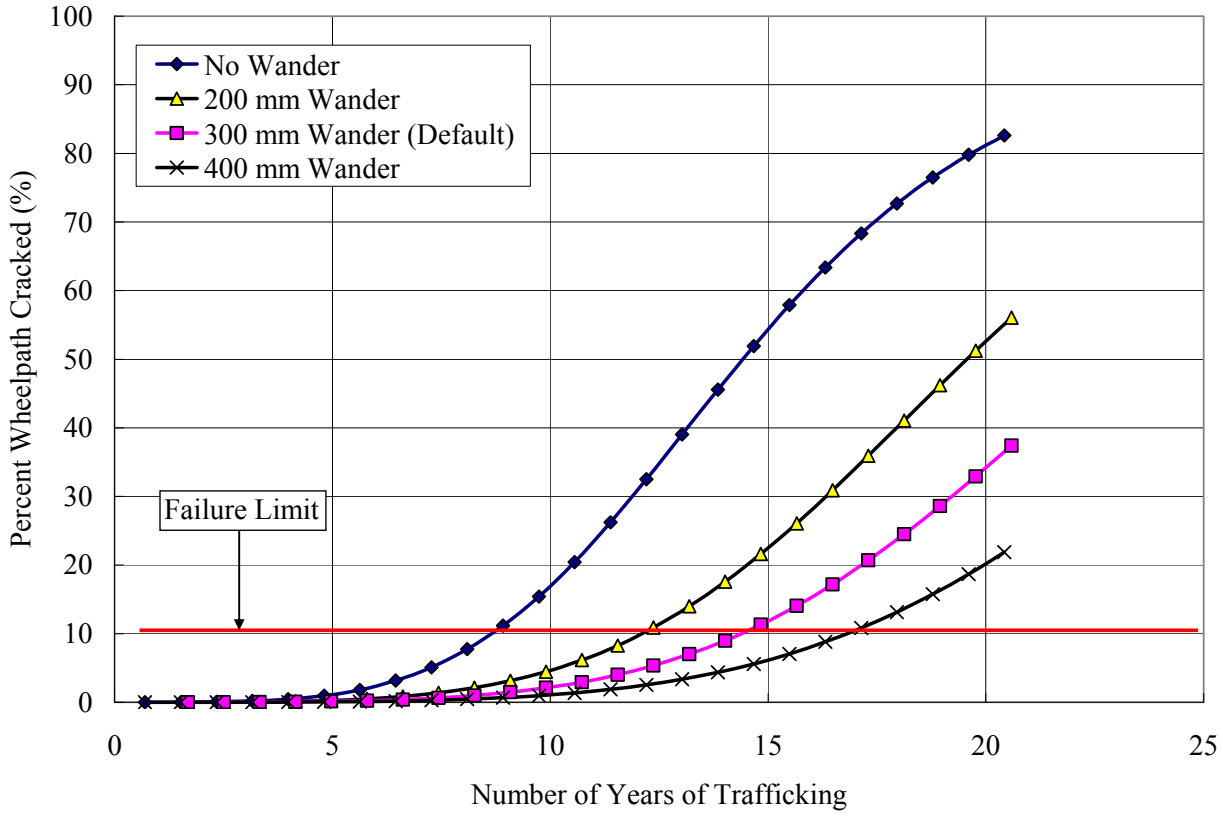

Figure 6.3: Effect of wander pattern on calculated surface cracking development, FSF = 0.14.

6.4 Effect of HMA Aging

Two aging settings were used to evaluate its effect on pavement fatigue cracking performance. The aging parameters defined in Equation (4) for the two cases, along with the corresponding pavement fatigue cracking lives are listed in Table 6.1. As shown in the table, pavement cracking life increases slightly, by about 5 percent, when HMA aging is included. It is therefore concluded that aging is not important for this project even though the aging model used tends to overpredict stiffness increase (see Section 4.3.3). Note that, as was shown in Section 4.3.3, the aging parameter was determined by assuming it would lead to a 25 percent increase over 10 years.

Table 6.1: Effect of HMA Aging on Pavement Fatigue Cracking Life

Case No.	Description	Value for A	Value for B	Fatigue Cracking Life (Year)
1	No Aging	0.0	1.0	8.3
2	With Aging	0.0305	1.0	8.7

6.5 Effect of Traffic Speed

Based on discussions presented in Section 4.4, traffic speed at the two MEF project sites ranges from 30 to 62.5 mph (48 to 101 km/hr) with heavier trucks traveling at lower speeds. The speed chosen for calibration was 35 mph (56 km/hr) to be weighted for the heavy trucks. This section evalutes the effect of traffic speed on pavement fatigue cracking life.

In this study, traffic speeds were varied from 30 to 70 mph (48 to 112 km/hr) at 10 mph (16 km/hr) intervals. The effect of traffic speed on pavement fatigue cracking life is shown in Figure 6.4. As the figure shows, traffic speed has almost no effect on fatigue cracking life: Reducing speed from 70 mph (112 km/hr) to 30 mph (48 km/hour) only reduces the life from 8.8 years to 8.6 years, a change of just 2 percent.

6.6 Effect of Traffic Volume

Uncertainties in the traffic volume originate from potential variations of the lane factor used in Equation (23) (Section 4.4). According to Reference *(12)*, the traffic pattern at WIM station number 020 can be classified into Group 1a, which has an average lane factor of 0.87 and varies between 0.53 and 0.97. The variation of fatigue life to 10 percent wheelpath cracking with lane factor for MEF-2 is shown in Figure 6.5. According to Figure 6.5, lane factor has a significant impact on the fatigue life of the pavement. Using a value of 0.87 for calibration may underestimate fatigue life by 36 percent or overestimate it by 10 percent in extreme cases.

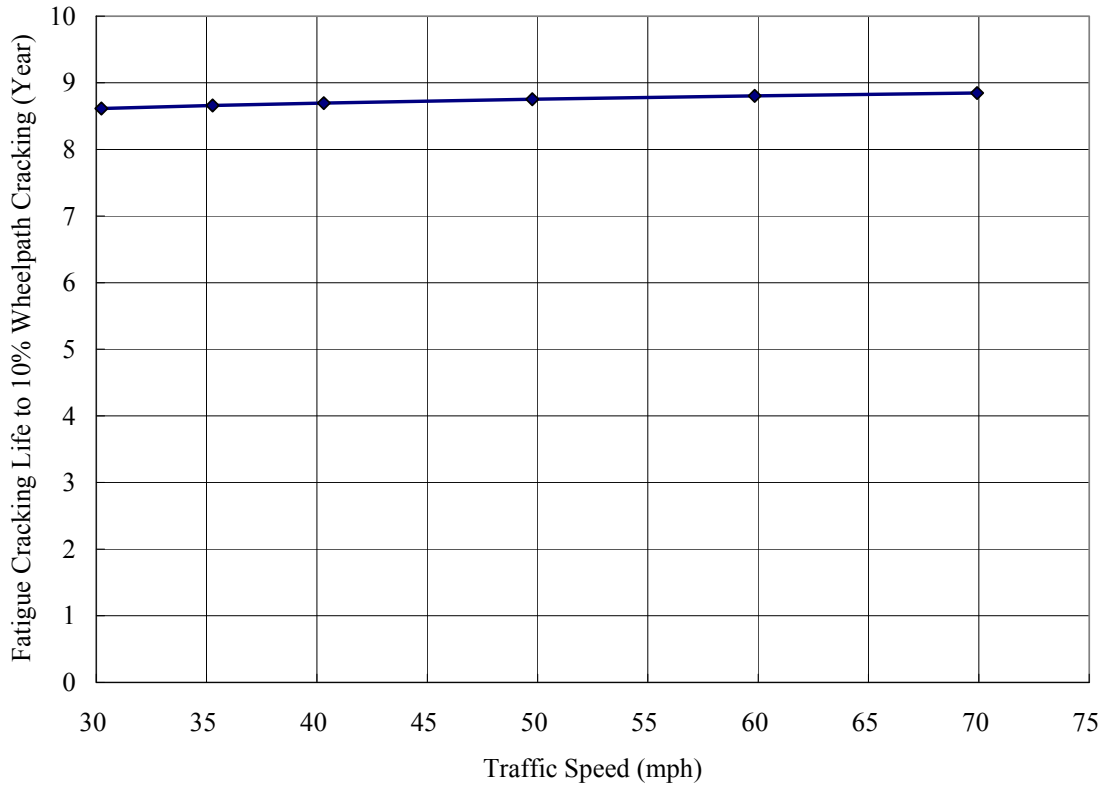

Figure 6.4: Effect of traffic speed on fatigue cracking life.

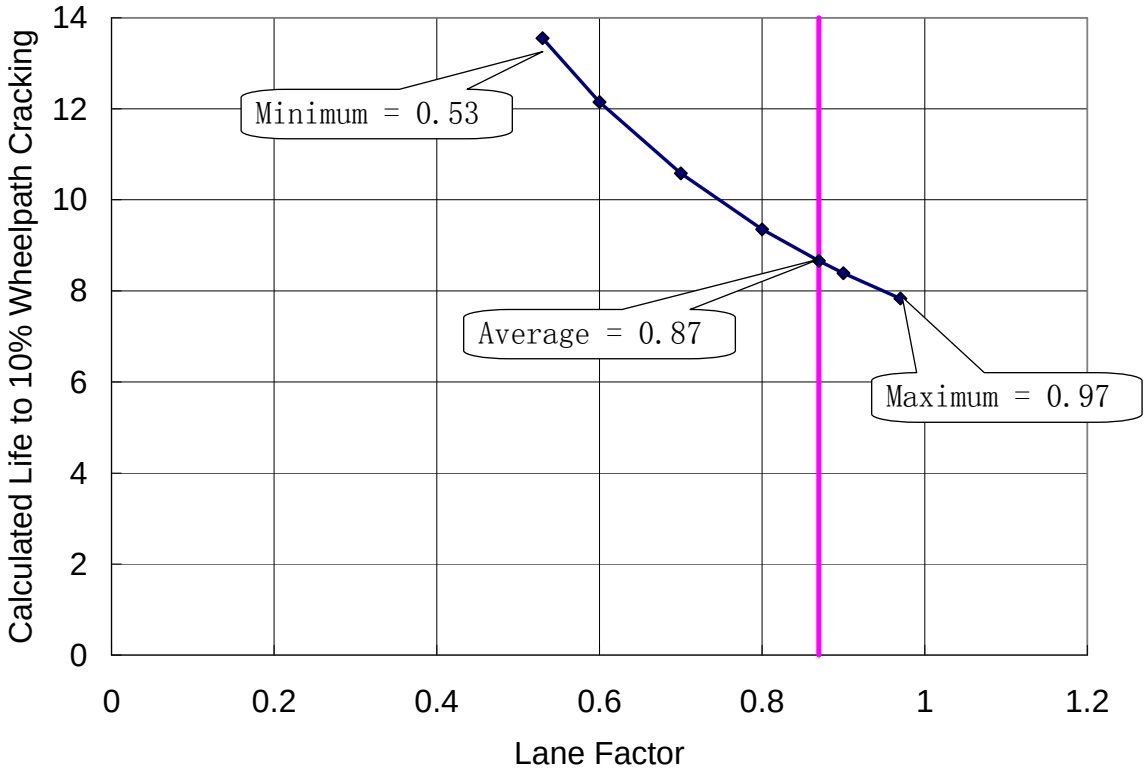

Figure 6.5: Variation of fatigue life to 10 percent wheelpath cracking with lane factor for MEF-2.

6.7 Sensitivity of Construction Variability

As mentioned in Section 4.3.2, the layer moduli for AB and TSG layers were found to have large variations based on the backcalculation results, and other layer moduli and thicknesses also have variances. It is therefore necessary to evaluate the sensitivity of pavement cracking life with respect to variations of the stiffness and thickness of various layers. This evaluation was accomplished using the "Variability—Monte Carlo Simulation" function in *CalME*. The variations in layer thicknesses, stiffnesses, and model parameters used for sensitivity analysis are listed in Table 6.2. As indicated in the notes, the variation of layer modulus was given based on backcalculation results, while others are default values provided by *CalME*.

Table 6.2: Variation in Layer Thickness and Modulus Used for Sensitivity Analysis

Layer Number	Description	COV of Thickness	SDF of Stiffness	SDF of *A* for Fatigue	SDF of *A* for Rutting
1	Original HMA surface	0.05	1.17*	1.2	1.15
2	ATPB + Aggregate Base (AB)	0.1*	1.23*	1.2	1.15
3	Top of subgrade (TSG)*	0	1.30*	1.2	1.15

*: These quantities were obtained from backcalculation of FWD data.
COV: Coefficient of variance.
SDF: Standard deviation factor, defined as 10 raised to the power of the standard deviation of the 10-based log of a quantity.

CalME performs Monte Carlo simulations based on the given variations in layer thicknesses and moduli. Various numbers of trials were used to determine the minimum number of trials required to reach converged mean and standard deviations for fatigue cracking life. The statistics are summarized in Table 6.3, which shows almost no difference between simulations with 20 and 30 trials when the "randomize" option is not checked. This indicates that 20 trials are enough to reach converged mean and standard deviations for fatigue cracking life in Monte Carlo simulation in *CalME*. Note that the 50^{th} percentile of fatigue cracking life converges to 8.8 years, which is practically the same as the 8.7 years obtained in the deterministic approach with mean inputs.

Table 6.3 also indicates that when Monte Carlo simulation is randomized, the results are quite different from those obtained when it is not randomized. However, judging from Figure 6.6, the empirical cumulative distribution functions (ECDF) of fatigue life for cases with or without randomization are quite similar. Accordingly, it was decided to run Monte Carlo simulation without randomization, thus avoiding the issues caused by the unpredictable nature of randomization.

ECDF can also be developed for crack initiation, which in *CalME* is assumed to be either 5 percent wheelpath cracking or 0.5 m/m^2 crack density. When ignoring surface crack propagation, the probability of crack initiation is the same as percent wheelpath cracking. Accordingly, the fatigue shift factor can alternatively be calibrated by matching the ECDF for crack initiation with the percent wheelpath cracking history.

Table 6.3: Statistics of Fatigue Cracking Life for Different Number of Trials (Unit: Year)

Number of Trials	Randomized?	50th Percentile	Average	Standard Deviation Factor
10	No	9.4	10.8	1.50
20	No	8.8	9.7	1.46
30	No	8.8	9.4	1.48
10	Yes	9.6	8.9	1.37
20	Yes	8.1	7.6	1.52
30	Yes	8.2	8.1	1.35

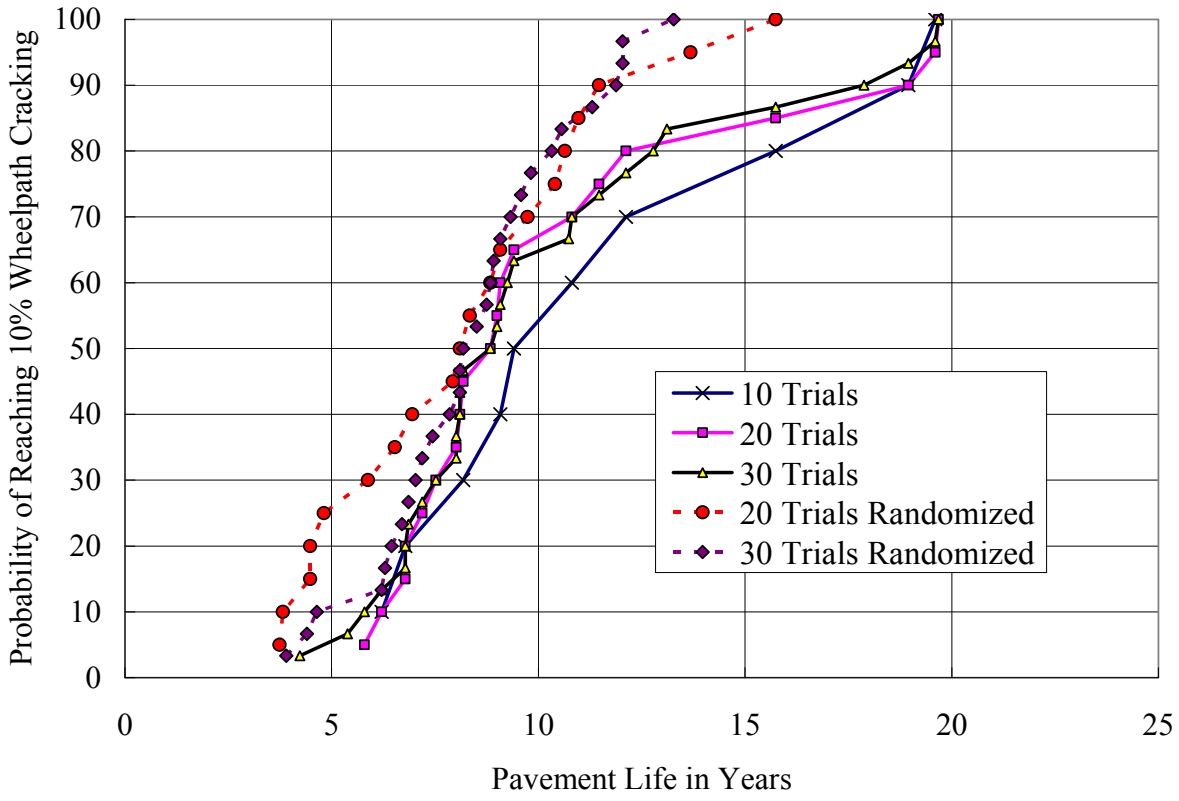

Figure 6.6: Empirical cumulative distribution functions of fatigue cracking life obtained from Monte Carlo simulations with different numbers of trials.

6.8 Determination of Fatigue Shift Factors with Deterministic Analysis

As shown in Section 4.5, measured surface cracking data for the MEF-2 and MEF-3 sections are provided on a yearly basis. With deterministic analysis, the mean values for all inputs are used and a crack density history can be calculated. The fatigue shift factor (FSF) is calibrated by adjusting its value to minimize the root mean square (RMS_{CR}) of the difference between calculated crack densities and observed values:

$$RMS_{CR} = \sqrt{\frac{1}{n}\sum_{i=1}^{n}(CR_{calculated} - CR_{observed})^2} \quad \textbf{(27)}$$

where: n is the number of years of crack density data, and
CR is the percentage of wheelpath cracking.

The number of years in Equation (27) is 8 for both MEF-2 and MEF-3, with the decreased crack density data discarded. The calibrated fatigue shift factors are listed in Table 6.4, along with the calculated fatigue cracking life to 10 percent wheelpath cracking for each project and RMS_{CR}. The "individual shift factors" in the table are the values needed to match the calculated and observed fatigue cracking life for each individual project. The comparison of the calculated and observed cracking development histories is shown in Figure 6.7, which shows good comparison between *CalME* predictions and observations for both MEF-2 and MEF-3.

Table 6.4: Calibrated Fatigue Shift Factors (FSF) for Deterministic Analysis

Project	HMA Stiffness	Wander	Individual Fitting		Average FSF
			FSF	RMS (%)	
MEF-2	FS	No	0.074	3.7	0.072
MEF-3	FS	No	0.069	2.2	
MEF-2	FS	Default	0.042	3.8	0.041
MEF-3	FS	Default	0.039	2.2	
MEF-2	FWD	No	0.081	3.7	0.080
MEF-3	FWD	No	0.078	2.1	
MEF-2	FWD	Default	0.047	3.7	0.046
MEF-3	FWD	Default	0.045	2.0	

Compared to the cases with default wander, it can be seen that the shift factor is roughly 1.74 to 1.76 times larger when wander is not allowed. Combined with the fact that fatigue life is about 1.70 times longer for cases with the default wander pattern when compared to cases without wander, it is believed that FSF for cases with default wander can be approximated by dividing the FSF for cases without wander by 1.70 (which is on the conservative side). This allows one to exclusively run cases without wander and to estimate the effects of wander from this conversion, which saves a lot of simulation time.

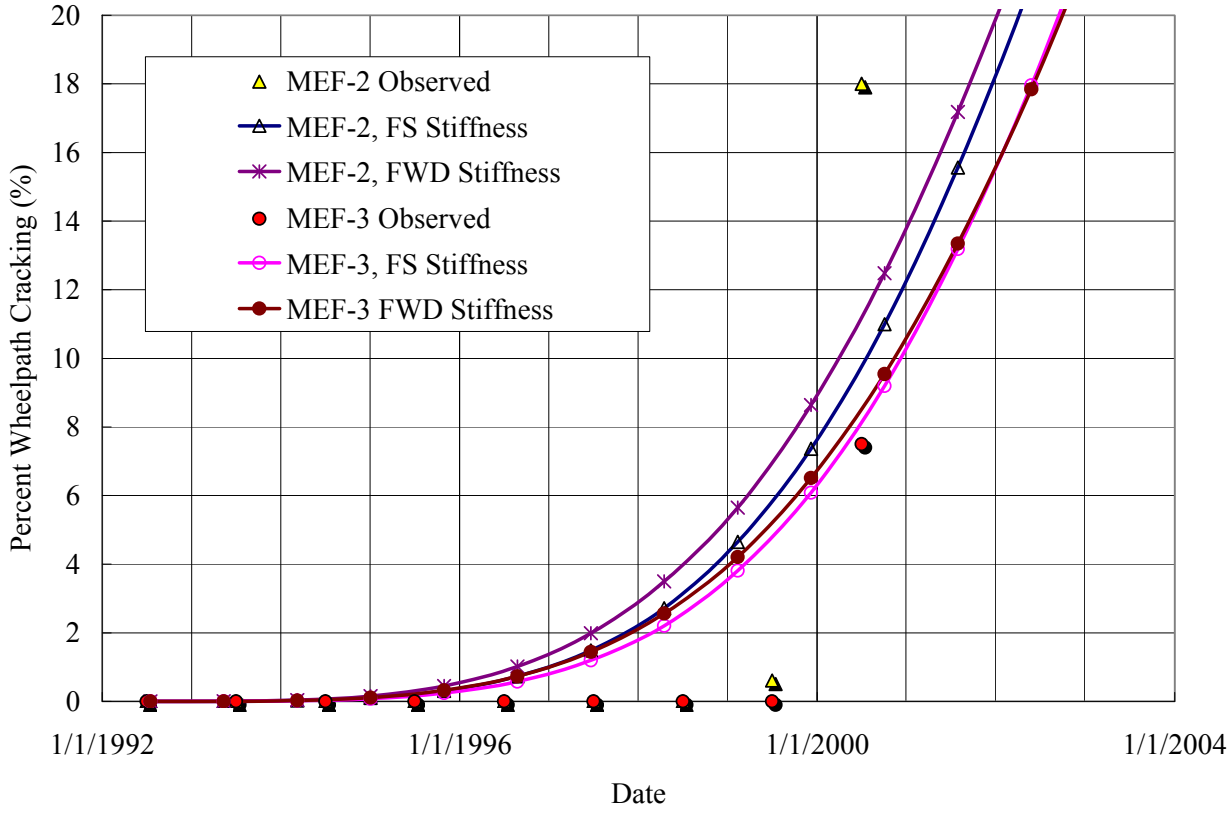

Figure 6.7: Comparison of calculated and observed wheelpath cracking, no wander allowed.

6.9 Determination of Fatigue Shift Factors with Probabilistic Analysis

As discussed in Section 6.7, the fatigue shift factor can be calibrated for probabilistic analysis by matching the ECDF (empirical cumulative distribution function) of crack initiation (defined as 5 percent wheelpath cracking) from Monte Carlo simulation with the percent wheelpath cracking history. Specifically, this is done by minimizing the same RMS_{CR} as in the deterministic analysis. The number of trials were set to 20 for each Monte Carlo simulation based on results presented in Section 6.7. A comparison of calculated ECDF for crack initiation with the observed surface cracking for MEF-2 using the FS stiffness for the HMA layer is shown in Figure 6.8, which indicates that the matching FSF is roughly 0.14. A similar plot for MEF-3 is shown in Figure 6.9, which indicates a matching FSF of 0.12.

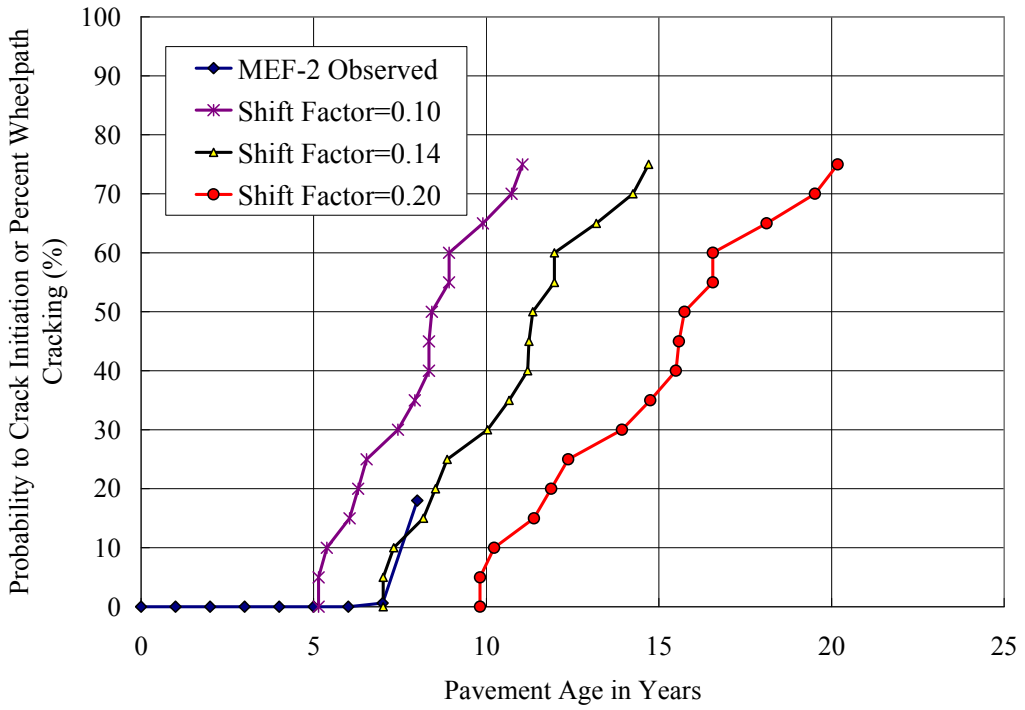

Figure 6.8: Comparison of observed cracking and ECDF for crack initiation for MEF-2 using FS stiffness for HMA layer, indicating a matching fatigue shift factor of 0.14.

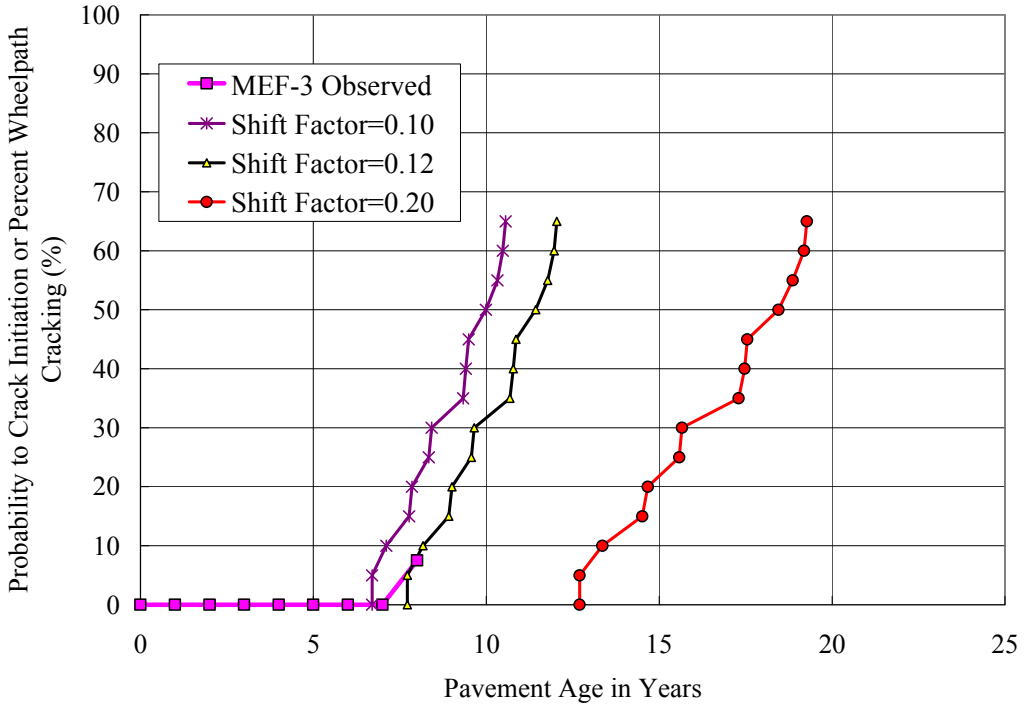

Figure 6.9: Comparison of observed cracking and ECDF for crack initiation for MEF-3 using FS stiffness for HMA layer, indicating a matching fatigue shift factor of 0.12.

Table 6.5: Calibrated Fatigue Shift Factors (FSF) for Probabilistic Analysis (Monte Carlo Simulation)

Project	HMA Stiffness	Wander	Individual FSF	RMS (%)	Overall FSF
MEF-2	FS	No	0.14	1.4	0.13
MEF-3	FS	No	0.12	0.5	
MEF-2	FS	Default	0.081*	-	0.075
MEF-3	FS	Default	0.070*	-	
MEF-2	FWD	No	0.14	3.3	0.14
MEF-3	FWD	No	0.14	0.027	
MEF-2	FWD	Default	0.081*	-	0.081
MEF-3	FWD	Default	0.081	0.12	

*: These shift factors were obtained by dividing the FSF for the no wander case by 1.7.

6.10 Rutting Performance Validation

Although rutting performance was not measured for the two US 101 projects, it was clear that no severe rutting was observed on the sites, according to the district materials engineer. Table 6.6 lists the calculated downward permanent deformation (DPD) for deterministic simulations for the two project sites and it shows that DPD ranged from 1.4 to 2.3 mm after 10 years of trafficking. This indicates that *CalME* predicted very little rutting in the pavements, which matches the observations.

Table 6.6: Calculated Downward Permanent Deformation (DPD)

Project	HMA Stiffness	Wander	Fatigue Shift Factor	Rutting Shift Factor	Calculated DPD after 10 years (mm)
MEF-2	FS	Default	0.074	1.4	1.71
MEF-3	FS	Default	0.069	1.4	1.63
MEF-2	FWD	Default	0.081	1.4	2.51
MEF-3	FWD	Default	0.078	1.4	2.40

6.11 Discussion

Based on the analyses and results presented above, the best overall fatigue shift factors range from 0.041 to 0.080 for deterministic analysis and from 0.075 to 0.14 for probabilistic analysis, depending on which types of stiffnesses are used for the HMA layer and whether wander is allowed in the traffic. This suggests that damage in the HMA material caused by one repetition in a bending beam fatigue test is equivalent to less than one pass of truck traffic in the field if all other conditions (e.g., strain and temperature) experienced by the material are the same. In other words, for deterministic analysis, highway traffic is roughly 12 to 24 times more damaging than laboratory bending beam action.

Note that there are some uncertainties about the input quantities that may affect the actual value of this fatigue shift factor. A summary of the uncertainties in the model inputs used is listed in Table 6.7.

Table 6.7: Summary of Uncertainties on Input Quantities

Quantity	Range Expected	Value Used	Potential Error Caused in Calculated Cracking Life
Wander Amount (mm)	200 to 400	300	±17%
Construction Variability	Typical values and backcalculation results	Various mean values	Standard deviation factor = 1.50
HMA Aging	With or without aging	-	±5%
Traffic Speed (mph)	30 to 70	35	±2%
Traffic Volume Determined by Lane Factor	0.53 to 0.97, mean 0.87	0.87	-36% for minimum, 10% for maximum

A comparison of fatigue shift factors calibrated for various projects are listed in Table 6.8. Note that the shift factor for US 101 projects corresponding to FS stiffness and deterministic analysis is also listed in Table 6.8 to be consistent with the inputs used by other studies. As the table shows, there is a large range for the fatigue shift factors used in different projects. The reason for this large range is unclear at this time and should be investigated with more calibration studies. Note that one should not expect the shift factor to be a constant; rather it should be a random variable. Part of this variability is accounted for in the Monte Carlo simulation by incorporating variability into *CalME* performance model parameters.

Table 6.8: Comparison of Fatigue Shift Factors Calibrated for Various Projects

Project	Mix Type	Fatigue Shift Factor	Reference
WesTrack	Fine and Fine Plus mixes	15	(2)
WesTrack	Coarse mixes	5	(2)
UCPRC HVS	Goal 1	3	(1)
UCPRC HVS	Goal 3 medium temp overlay	3	(1)
UCPRC HVS	Goal 3 medium temp underlying	0.6	(1)
UCPRC HVS	Goal 3 high temp	3	(1)
UCPRC HVS	Goal 5	3	(1)
UCPRC HVS	Goal 9 underlying layer	3	(1)
US 101	Original HMA	0.041	This report, Table 6.4

7 CONCLUSIONS AND RECOMMENDATIONS

This technical memorandum presents calibration of fatigue shift factors for HMA materials using data collected from two sites on US 101 in Humboldt County, California (PM 127.5 and PM 129.9).

The overall shift factor was found to be 0.072 for deterministic analysis and 0.13 for probabilistic analysis (Monte Carlo simulation) under typical design scenarios (i.e., with stiffness determined from frequency sweep testing and without traffic wander in order to save simulation time), don't allow traffic wander to save simulation time), which indicates that highway traffic is more damaging than bending beam action in the laboratory. Specifically, one load cycle in the bending beam fatigue test is equivalent to 0.072 to 0.13 truck axle passes in the field, if the strain and other conditions are the same. It was found that *CalME* predicts 70 percent longer fatigue life when traffic wander is allowed compared to when wander is not allowed.

These shift factors were obtained based on data collected in year 2007, which was five years after the original flexible pavement was overlaid with HMA pavement and an OGFC wearing course. Although the input data are believed to represent the actual field conditions, the combined uncertainties of the quantities may lead to significant errors in the worst case. The factors that have the most significant impact on the simulation results are construction variability and lane factor. Uncertainties in each of these factors can lead to a 40 percent error in calculated fatigue life for the two projects on US 101.

Using a shift factor of 1.4 for K for the HMA rutting model determined from the previous calibration study using HVS data *(1)*, *CalME* predicted very little downward permanent deformation for the two project sites. These predictions are consistent with the observation made by the district materials engineer.

It was found that the fatigue shift factor calibrated in this study is quite different from those reached in previous calibration studies using HVS and WesTrack test data (see *[1]* and *[2])*. It is recommended that the shift factor calibrated in this memo be verified with more studies, including calibration studies and validation studies.

REFERENCES

1. Ullidtz, P., Harvey, J.T., Tsai, B.-W., and Monismith, C.L. 2006. *Calibration of Incremental-Recursive Flexible Damage Models in CalME Using HVS Experiments.* Report prepared for the California Department of Transportation (Caltrans) Division of Research and Innovation, University of California Pavement Research Center, Davis and Berkeley. UCPRC-RR-2005-06.
2. Ullidtz, P., Harvey, J., Tsai, B.-W., and Monismith, C.L. *Calibration of CalME Models Using WesTrack Performance Data.* 2007. Report prepared for Caltrans Division of Research and Innovation and Caltrans District 8 by the University of California Pavement Research Center, Davis and Berkeley. UCPRC-RR-2006-14.
3. *Guide for Mechanistic-Empirical Design of New and Rehabilitated Pavement Structures.* 2004. National Cooperative Highway Research Program, Transportation Research Board, National Research Council.
4. Deacon, J.A., Harvey, JT., Guada, I., Popescu, L., and Monismith, C.L. 2002. *Analytically Based Approach to Rutting Prediction.* Transportation Research Board, 2002. 1806.
5. Guada, I., Signore, J., Tsai, B.-W., Jones, D., Harvey, J., and Monismith, C.L. 2007. *Reflective Cracking Study: First-Level Report on Laboratory Shear Testing.* Report prepared for Caltrans Division of Research and Innovation by the University of California Pavement Research Center, Davis and Berkeley. UCPRC-RR-2006-11.
6. Ongel, A. and Harvey, J.T. 2004. *Analysis of 30 Years of Pavement Temperatures using the Enhanced Integrated Climate Model (EICM).* Draft report prepared for the California Department of Transportation. Pavement Research Center, Institute of Transportation Studies, University of California Berkeley, University of California Davis. UCPRC-RR-2004-05.
7. Jones, D., et al., *Full-Depth Pavement Reclamation with Foamed Asphalt: Final Report.* 2008, University of California Pavement Research Center.
8. Harvey, J. and B.-W. Tsai. 1997. *Long-Term Oven-Aging Effects on Fatigue and Initial Stiffness of Asphalt Concrete*. Transportation Research Record 1590: p. 89–98.
9. Bell, C.A., *Summary Report on the Aging of Asphalt-Aggregate Systems.* 1989. Strategic Highway Research Program (SHRP) Publications, SHRP-A-305. Oregon State University: 100.
10. Moore, Jr., R.L. 1989. *Structural Value of Asphalt Treated Permeable Base and Open Graded Asphalt Concrete*. FHWA/CA/TL-89/11. Division of New Technology, Transportation Materials & Research—California Department of Transportation Sacramento, California 95809.
11. Harvey, J., Tsai, B.-W., Long, F., and Hung. D. 1999. *CAL/APT Program: Asphalt Treated Permeable Base (ATPB), Laboratory Tests, Performance Predictions and Evaluation of Caltrans and Other Agencies Experience.* Report prepared for the California Department of Transportation. Pavement Research Center, CAL/APT Program, Institute of Transportation Studies, University of California, Berkeley. UCPRC-RR-1999-05.

12. Lu, Q. 2008. *Estimation of Truck Traffic Inputs Based on Weigh-in-Motion Data in California.* 2008: Technical memorandum prepared for California Department of Transportation Division of Research and Innovation, Office of Roadway Research by the University of California Pavement Research Center, Berkeley and Davis. UCPRC-TM-2008-08.
13. Kannekanti, V., Lee, C., Popescu, L., Harvey, J.T., and Nokes, W. 2007. *Pavement Performance Data Extraction from the Caltrans PMS*. Technical memorandum prepared for the California Department of Transportation Division of Research and Innovation Office of Roadway Research by the University of California Pavement Research Center, Berkeley and Davis. UCPRC-TM-2007-06.
14. Stempihar, J.J., Williams, R.C., and Drummer, T.D. 2009. *Quantifying Lateral Displacement of Trucks for Use in Flexible Pavement Design.* Presented at the 88th Annual Meeting of the Transportation Research Board, January 11 to 15, 2009.